



## Dual origin of Fe–Ti–P gabbros by immiscibility and fractional crystallization of evolved tholeiitic basalts in the Sept Iles layered intrusion

Olivier Namur <sup>a,\*</sup>, Bernard Charlier <sup>b</sup>, Marian B. Holness <sup>a</sup>

<sup>a</sup> Department of Earth Sciences, University of Cambridge, CB2 3EQ Cambridge, United Kingdom

<sup>b</sup> Massachusetts Institute of Technology, Department of Earth, Atmospheric, and Planetary Sciences, Cambridge, MA 02139-4307, USA

### ARTICLE INFO

#### Article history:

Received 20 April 2012

Accepted 30 June 2012

Available online 11 July 2012

#### Keywords:

Ferrogabbro  
Liquid immiscibility  
Silicate liquid  
Forward model  
Pigeonite  
Unmixing

### ABSTRACT

We present a detailed study of two ca. 200 m-thick apatite-bearing ferrogabbro horizons of the Sept Iles layered intrusion (Canada). These rocks are the most evolved cumulates of the megacyclic units (MCU) I and II, and mark the transition between basaltic and silicic magmatism. They are made up of plagioclase ( $An_{55-34}$ ), olivine ( $Fo_{66-21}$ ), clinopyroxene (Mg#75–55), ilmenite, magnetite, apatite,  $\pm$  pigeonite and are a significant source of Fe–Ti–P ore. Ferrogabbros have relatively uniform bulk-rock compositions in MCU I but are bimodal in MCU II. The liquid lines of descent for major elements in equilibrium with cumulates of MCU I and II have been calculated using a forward model formalism. Both trends evolve towards  $SiO_2$ -enrichment and  $FeO_t$ -depletion after saturation in Fe–Ti oxides. However, because of magma mixing in MCU II, they do not follow the same path. Evolved liquids from MCU II are shown to enter the experimentally-determined two liquid stability field, while MCU I liquids do not. Immiscibility in MCU II and its absence in MCU I are supported by the presence of contrasted reactive symplectites in cumulate rocks. Apatite-bearing ferrogabbros in MCU II have crystallized from distinct immiscible Fe-rich and Si-rich silicate melts which have physically segregated in the slow-cooling magma chamber. Two different types of cumulate rocks are thus produced: leucocratic and melanocratic gabbros. This is consistent with the presence of Si-rich and Fe-rich melt inclusions in apatite. In contrast, homogeneous ferrogabbros from MCU I were produced by simple fractional crystallization of a homogeneous liquid. Our data suggest that immiscibility could also explain the large geochemical variability of ferrogabbros in the Upper Zone of the Bushveld Complex (South Africa).

© 2012 Elsevier B.V. All rights reserved.

### 1. Introduction

Fe–Ti–P gabbros are common cumulate rocks crystallized from tholeiitic basalts. Thick horizons of gabbro dominated by Fe–Ti oxides and apatite are observed in various layered intrusions such as Bushveld, Skaergaard, Bjerkreim-Sokndal, Duluth and Panzhihua (Duchesne and Charlier, 2005; Eales and Cawthorn, 1996; Higgins, 2005; Miller and Ripley, 1996; Namur et al., 2010; Ripley et al., 1998; Tegner et al., 2006; Zhou et al., 2005). Ferrogabbros are also commonly associated with massif-type anorthosites (e.g. Duchesne et al., 2006; Dymek and Owens, 2001; Zhao et al., 2009). Occurrences in subvolcanic–volcanic environment (Kiruna-type deposits; Harlov et al., 2002) and in the lower oceanic crust have also been reported (Dick et al., 2000; Natland et al., 1991). The origin of these rocks has been variously suggested to result from crystal fractionation associated with density-driven mineral sorting (e.g. Charlier et al., 2008; Tegner et al., 2006; Tollari et al., 2008; Wager and Brown, 1968) or crystallization

of an Fe–Ti–P-rich silicate melt segregated from its Si-rich immiscible conjugate (e.g. Bateman, 1951; Harlov et al., 2002; Naslund, 1983; Philpotts, 1967). However, Charlier et al. (2011) and Jakobsen et al. (2011) have shown that evolved Fe–Ti–P gabbros from the Skaergaard and Sept Iles layered intrusions have crystallized from a liquid emulsion. The question concerning the origin of these rocks is thus not whether they are cumulates or solidified immiscible liquids but if they are cumulates formed from a homogenous melt or from a mixture of immiscible liquids.

In this contribution, we present a detailed study of two ca. 200 m-thick horizons of magnetite, ilmenite and apatite-rich gabbros in the Sept Iles layered intrusion (Canada). One occurs in the lower part of the intrusion and the other one in the middle part. Both horizons are the most evolved cumulates of their respective megacyclic unit (MCU). The lowermost gabbro horizon is very homogeneous, comprising moderately leucocratic (plagioclase-rich) rocks with ca. 5 wt.% of apatite (av. 2.5 wt.%  $P_2O_5$ ; Namur et al., 2010). The uppermost gabbro horizon is more heterogeneous and contains layers of gabbro dominated by Fe–Ti oxides, ferromagnesian minerals and apatite (ca. 20 wt.% of apatite) that alternate with very plagioclase-rich gabbros depleted in mafic minerals and apatite (ca. 2 wt.% of apatite)

\* Corresponding author. Tel.: +44 1223 333434; fax: +44 1223 333450.

E-mail address: [obn21@cam.ac.uk](mailto:obn21@cam.ac.uk) (O. Namur).

on a scale of 5 to 20 m (Charlier et al., 2011). Using new mineral and whole-rock data of these rocks together with those presented in Charlier et al. (2011) and Namur et al. (2010), and modeling of the liquid line of descent, we show that the fractionation path followed, and the processes that occur, during differentiation are critical in determining the extent of Fe–Ti–P enrichment. The compositional evolution of the melt controls whether the Fe–Ti–P gabbros form by fractional crystallization of a homogeneous melt or of a mixture of immiscible liquids. Late-stage microstructures in cumulate rocks from the Skaergaard intrusion have recently been studied by Holness et al. (2011). Various types have been described among which oxy-symplectites (comprising orthopyroxene and magnetite) and Type 2 symplectites (comprising orthopyroxene and plagioclase) were attributed to reaction between a homogeneous melt and cumulus phases, while Type 1 symplectites (Fe–Ti oxide-rooted symplectites dominated by clinopyroxene, olivine and plagioclase) were attributed to reaction between cumulus primocrysts and an Fe-rich immiscible liquid (Holness et al., 2011). We use the

stratigraphic distribution of similar microstructures in the Sept Iles intrusion to determine when immiscibility occurred during progressive crystallization.

## 2. The Sept Iles layered intrusion

The Sept Iles layered intrusion is located on the north shore of the St Lawrence River, about 500 km to the north-east of Quebec City. It is an unmetamorphosed and undeformed magmatic body, emplaced at  $564 \pm 4$  Ma (U–Pb on zircon; Higgins and van Breemen, 1998) into high-grade gneisses of the Grenville Province. The intrusion has a dinner-plate shape with a diameter of ca. 80 km, a maximum thickness of ca. 5.5 km and an estimated magma volume of ca.  $20,000 \text{ km}^3$  (Loncarevic et al., 1990). The north-western part of the intrusion crops out around the Sept Iles peninsula and on islands of the Sept Iles archipelago, where three different series have been described: the Layered Series, the Upper Border Series and the Upper Series (Fig. 1A; Higgins, 2005).

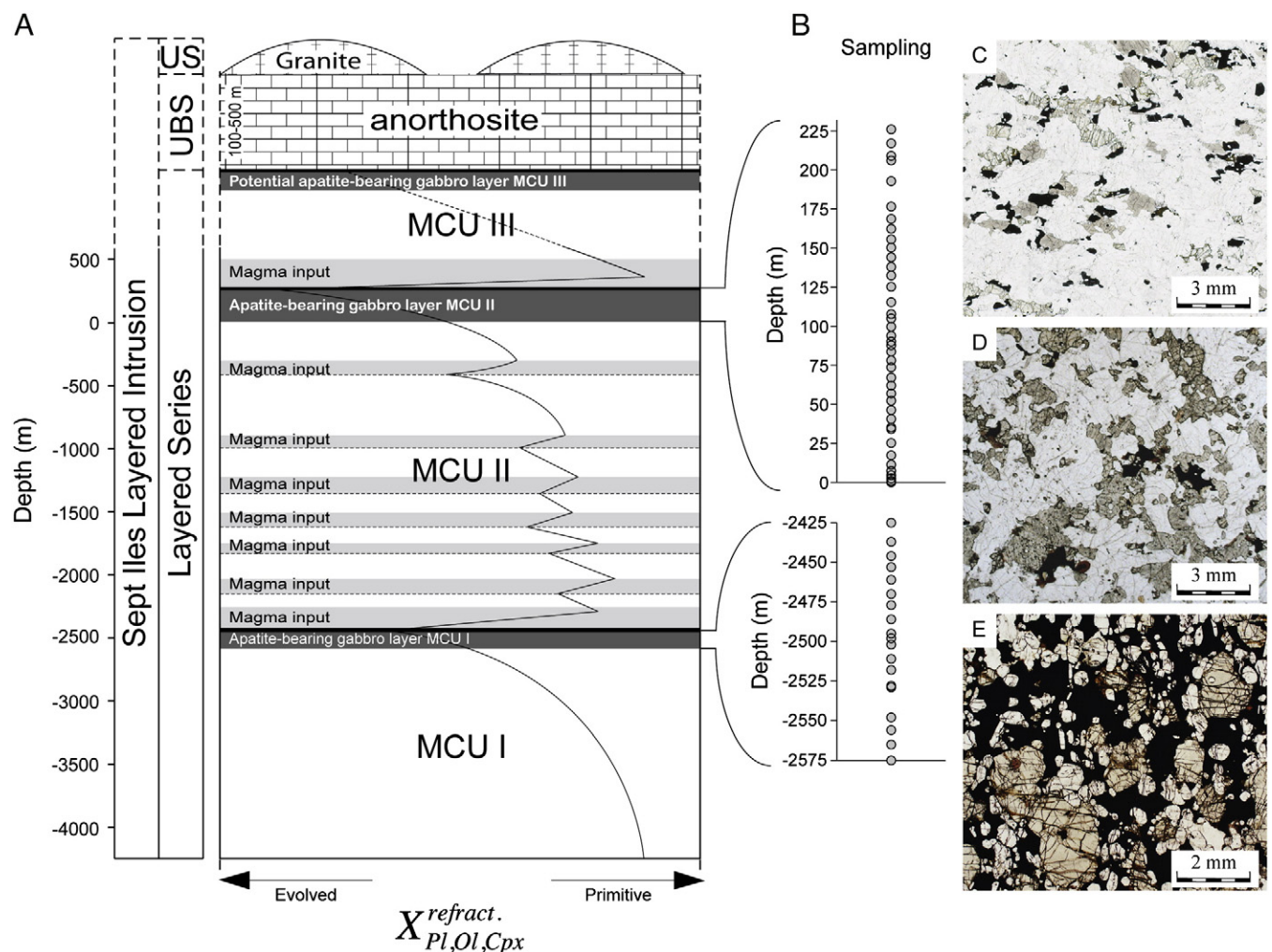


**Fig. 1.** Schematic stratigraphy of the Sept Iles layered intrusion, stratigraphic position of the samples and petrography of the Fe–Ti–P gabbro horizons. A. Stratigraphic subdivision of the intrusion (after Namur et al., 2010). The “0-meter” reference level corresponds to the appearance of cumulus apatite in Megacyclic Unit 2 (MCU II). Curves display schematically the evolution of mineral compositions (Pl: Plagioclase An-content; Ol: Olivine Fo-content, Cpx: Clinopyroxene Mg#; Mt: Magnetite Cr-content). Light grey bands in MCU II and at the base of MCU III represent mixing zones between residual liquid and new magma inputs. UBS: Upper Border Series; US: Upper Series. B. Stratigraphic intervals of the Fe–Ti–P gabbro horizons (MCU I and MCU II) investigated in this study. Stratigraphic positions of the samples from drill cores (DC9; s9) and surface samples are indicated. C. Photomicrograph of a representative Fe–Ti–P gabbro from the apatite-bearing horizon of MCU I. Sample DC9-419; transmitted light. D. Photomicrograph of a representative Fe–Ti–P-poor gabbro from the apatite-bearing horizon of MCU II. Sample s9-88.1; transmitted light. E. Photomicrograph of a representative Fe–Ti–P-rich gabbro from the apatite-bearing horizon of MCU II. Sample s9-148; transmitted light.

The ca. 4.7 km-thick Layered Series is made up of 3 megacyclic units (MCU) showing the following succession of cumulus assemblages: troctolite (plagioclase and olivine; po-C; classification following Irvine, 1982), Fe-Ti oxide-bearing troctolite (plagioclase, olivine, Fe-Ti oxide minerals; pomi-C) and layered gabbro (plagioclase, Fe-Ti oxide minerals, clinopyroxene, ± olivine, ± apatite; pomic-C; pmic-C; pomica-C; Namur et al., 2010). Each megacyclic unit results from the crystallization of a new influx of ferrobasaltic parent magma (Namur et al., 2010, 2011a). Additionally, six minor magma chamber replenishments occurred during the crystallization of MCU II (Fig. 1A). The Sept Iles Layered Series is characterized by the presence of abundant cm- to m-scale anorthositic blocks (autoliths) included in gabbroic rocks (Higgins, 2005) and resulting from anorthosite from the roof of the intrusion sinking in relatively low-density Fe-Ti oxide saturated melts (Namur et al., 2011b).

The 100–500 m-thick Upper Border Series is made up of anorthosite, with minor leucotroctolite and leucogabbro (Higgins, 1991). It also contains many cm- to dm-scale pods of granophyre (syenite to granite) resulting from liquid percolation through the plagioclase + liquid mush (Namur et al., 2011a). This unit has been shown to result from accumulation of buoyant plagioclase at the roof of the magma chamber by flotation on Fe-Ti oxide unsaturated melts (Namur et al., 2011b).

The Upper Series is made up of ferroan metaluminous syenite and granite with minor monzonite (Higgins and Doig, 1986; Namur et al., 2011a). It forms small cupolas topping the central part of the intrusion. Namur et al. (2011a) have shown that rocks from the Upper Series represent evolved residual liquids left after extensive fractionation of the Layered Series and the Upper Border Series from the Sept Iles ferrobasaltic parent magma.

### 3. Sampling and analytical methods

Twenty samples were collected from the apatite-bearing gabbro horizon of MCU I at stratigraphic heights ranging from –2575 to –2425 m, with the “0 meter” reference level defined as the lowest sample containing cumulus apatite in MCU II (Fig. 1B). The apatite-bearing MCU I horizon is mostly unlayered and homogeneous, and we took representative samples (each 40–50 cm-long) from the 46.2 mm diameter drill-core BH84699 (DC-9) drilled by Inco Inc, and kept at the Ministère des Ressources Naturelles et de la Faune du Québec. The true stratigraphic position and the distance between samples have been corrected for the average local dip of the igneous layering, estimated at 30° south. Forty-one samples were collected from the apatite-bearing gabbro horizon of MCU II at stratigraphic heights ranging from 0 to 252 m (Fig. 1B). Thirty-five of these (each 40–50 cm long) come from the drill-core 1166-95-09 (s9) drilled by the Soquem Inc., perpendicular to the igneous layering with an inclination of 65° and an azimuth of 325°. The others are 6 surface samples (ca. 4 kg) collected during 2007. The positions of the surface samples were precisely determined from global positioning system (GPS) coordinates and altimeter data. The apatite-bearing gabbro horizon of MCU II is significantly layered, with apatite- and Fe-Ti oxide-rich rocks alternating with plagioclase-rich and mafic mineral-poor layers on a scale of ca. 20 m at the base decreasing to ca. 5 m at the top. Representative samples of both types of layers have selected for this study.

All the samples were carefully brushed and water-cleaned prior to crushing. They were manually crushed with a hammer and milled with agate mortars. Whole-rock compositions were obtained by XRF using an ARL 9400XP spectrometer at the University of Liege (Belgium). Major elements were measured on lithium tetra- and meta-borate fused glass discs, with matrix correction following the Traill-Lachance algorithm. Trace elements and phosphorous were measured on pressed powder pellets and data were corrected for matrix effects by Compton peak monitoring. Accuracy is estimated as

better than 1% for major elements and 5% for trace elements, and was controlled using 40 international and in-house standards.

Plagioclase separations (80–150 µm) were performed using flotation in bromoform and magnetic separation (Frantz isodynamic separator). Final purification was achieved by HCl leaching of mineral separates to dissolve any grains of apatite, followed by thorough cleaning of the mineral powders in ultrapure water and manual grinding in an agate mortar. Major element compositions were obtained by XRF of Li-fused glass discs.

The major element compositions of olivine and pyroxenes were obtained using a Cameca SX 100 electron microprobe at the University of Clermont-Ferrand (France). Analytical conditions were 15 kV for the accelerating voltage, 15 nA for the beam current and a focused beam. When possible, at least three points in the cores of each of three grains were measured and the values reported here correspond to the mean of all the measurements. The following standards were used for K $\alpha$  X-ray lines calibration: wollastonite for Si and Ca, Al<sub>2</sub>O<sub>3</sub> for Al, fayalite for Fe, forsterite for Mg, MnTiO<sub>3</sub> for Mn and Ti, albite for Na and orthoclase for K. Raw data were corrected with the CATZAF software.

Mineral modes were determined by point-counting on polished thin-sections. At least 1000 points were counted for each sample on a grid of 0.4×0.4 mm. The estimated accuracy is better than 5% at the 99% confidence level (Howarth, 1998). The data obtained in volume percent were converted to weight percent using the density of the minerals calculated from their chemical compositions.

Bulk-rock density was determined for 20 samples from the apatite-bearing gabbro horizon of MCU I and for 266 samples from the apatite-bearing horizon of MCU II (Charlier et al., 2011). Densities were measured by weighing the dry, clean sample in air and then in water, following Archimedes' principle. The precision is estimated to be 1–2% relative.

### 4. Fe-Ti-P gabbros in the Layered Series

#### 4.1. Petrography

The 150 m-thick apatite-bearing gabbro horizon of MCU I comprises very homogeneous equi- to hetero-granular, and medium-grained (1–5 mm) unlayered rocks (Fig. 1C). Plagioclase, olivine, clinopyroxene, magnetite, ilmenite and apatite are the most abundant minerals, with subordinate K-feldspar, biotite, amphibole and Fe–Cu–Ni sulfides (chalcopyrite, pyrite and pyrrhotite). Plagioclase (40–62 wt.%; Fig. 2A; Supplementary Material 1) is ubiquitous, forming sub-equant to strongly tabular subhedral to euhedral grains. It is generally unzoned and defines a strong magmatic lamination in most samples. Olivine (9–26 wt.%) is represented by equant to slightly prismatic subhedral to euhedral grains. Clinopyroxene (6–18 wt.%) occurs as subhedral to euhedral prismatic grains oriented parallel to the magmatic lamination defined by the plagioclase and is frequently twinned. Iron-titanium oxide minerals are represented by both the magnetite-ulvöspinel solid-solution (2–13 wt.%) and the ilmenite-hematite solid solution (4–12 wt.%). These minerals have crystallized as polycrystalline anhedral aggregates, generally weakly dominated by magnetite. Apatite (4–8 wt.%) forms euhedral mm-sized grains. A single type of brownish multiphase solid inclusions (50–200 µm) is common in apatite grains: they have negative crystal shapes, suggesting that they represent crystallized entrapped melts.

The 252 m-thick apatite-bearing gabbro horizon of MCU II is made up of equi- to hetero-granular and medium- to coarse-grained (1–5 mm) rocks with the same minerals as those of the apatite-bearing gabbro horizon of MCU I, with the major difference being the presence of abundant pigeonite. Two main types of gabbro alternate stratigraphically on a scale of 5–20 m: (1) Leucocratic gabbro (Fig. 1D) dominated by subhedral to euhedral unzoned and tablet-shaped plagioclase (44–71 wt.%; Fig. 2B), equant to slightly

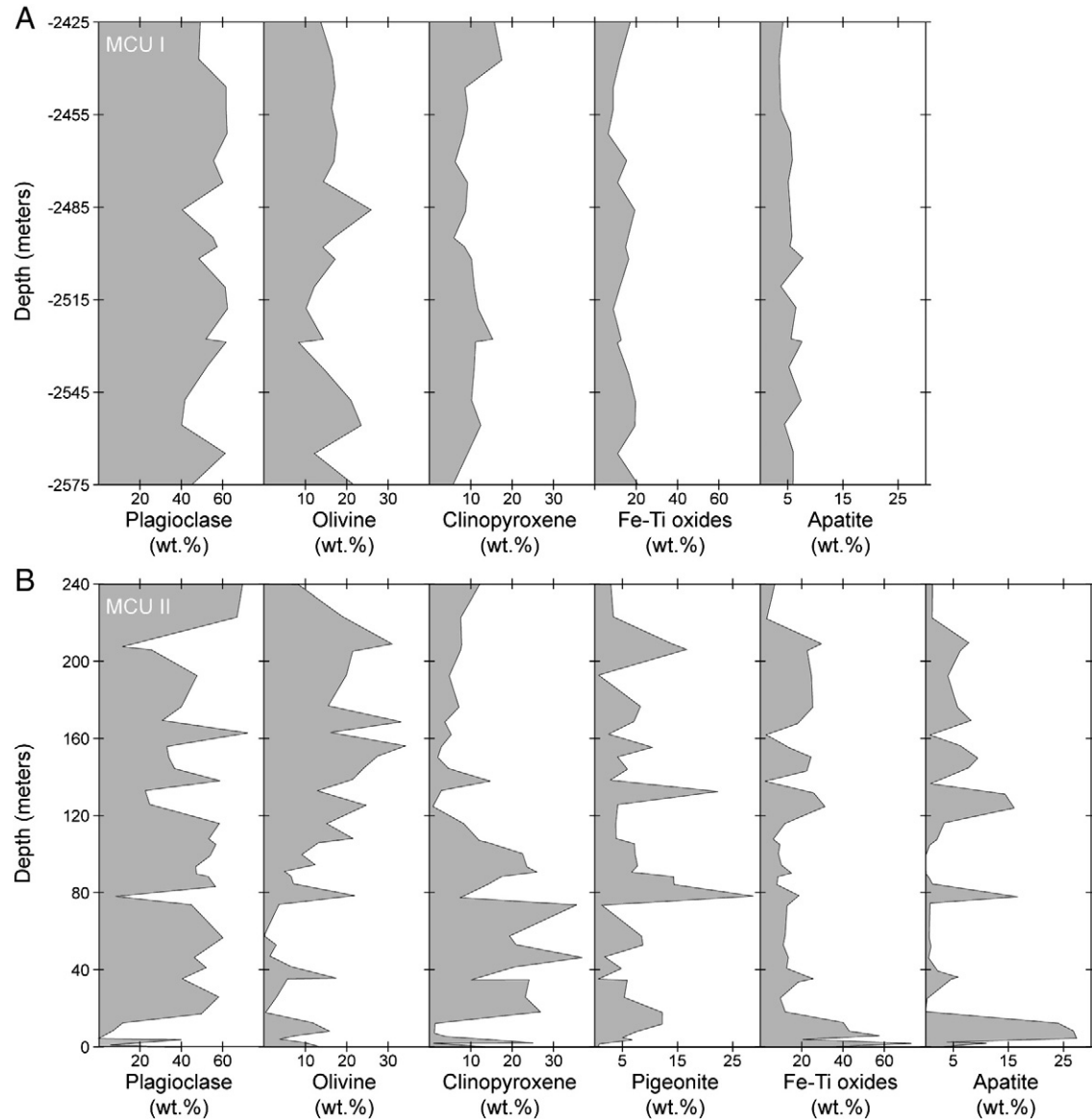


**Fig. 2.** Mineral modes (wt.%) in Fe-Ti-P gabbro horizons of the Sept Iles intrusion. A. MCU I. B. MCU II. Mineral modes have been determined by point-counting on polished thin sections (>1000 points per sample) and converted to wt.% using appropriate mineral densities.

prismatic olivine (0–22 wt.%), tabular clinopyroxene (5–38 wt.%), pigeonite (1–13 wt.%) and anhedral Fe-Ti oxides from both the magnetite-ulvöspinel solid solution (1–12 wt.%) and the ilmenite-hematite solid solution (2–9 wt.%). Apatite is present in relatively low amounts (0.1–3.5 wt.%) and has crystallized as mm-scale euhedral grains; (2) Melanocratic gabbro (Fig. 1E) dominated by Fe-Ti oxides (magnetite-ulvöspinel: 6–40 wt.%; ilmenite-hematite: 6–32 wt.%; Fig. 2B), olivine (4–34 wt.%), clinopyroxene (0–25 wt.%), pigeonite (0–27 wt.%) and apatite (3–28 wt.%). The proportion of plagioclase ranges from 1 to 47 wt.%, but is generally lower than 35 wt.% and globally increases from base to top of the 250 m-thick apatite-bearing gabbro horizon. In most samples, there is more olivine than clinopyroxene compared to the leucocratic gabbros. Apatite grains from both types of MCU II gabbro contain abundant multiphase solid inclusions with negative shape and interpreted as representing crystallized melt inclusions (Charlier et al., 2011). Two types of inclusion are observed, one dark (50–120  $\mu\text{m}$ ) and the other light (10–80  $\mu\text{m}$ ).

#### 4.2. Mineral compositions

In the apatite-bearing gabbro horizon of MCU I, major element mineral compositions show a continuous evolution from base to top with plagioclase (An: molar  $100[\text{Ca}/(\text{Ca} + \text{Na})]$ ) ranging from  $\text{An}_{51}$  to  $\text{An}_{47}$  (Supplementary Material 2), olivine (Fo: molar  $[\text{Fe}/(\text{Fe} + \text{Mg})]$ ) from  $\text{Fo}_{61}$  to  $\text{Fo}_{55}$  (Supplementary Material 3) and clinopyroxene (Mg#: molar  $[\text{Fe}/(\text{Fe} + \text{Mg})]$ ) from Mg# $_{71}$  to Mg# $_{69}$  (Supplementary Material 4; Fig. 3). A reverse trend of plagioclase, olivine and clinopyroxene composition to  $\text{An}_{51}$ ,  $\text{Fo}_{66}$  and Mg# $_{74}$  is observed at the top of MCU I (defined by the disappearance of cumulus apatite; Fig. 3) and results from a large magma chamber replenishment event by undifferentiated basalt (Namur et al., 2010). This reversal extends to  $\text{An}_{65}$ ,  $\text{Fo}_{67}$  and clinopyroxene-Mg# $_{77}$  in apatite-free gabbros from the base of MCU II (Namur et al., 2010; Fig. 1A).

In the apatite-bearing gabbro horizon of MCU II, major element mineral compositions also show a continuous evolution from base to top with plagioclase decreasing continuously from  $\text{An}_{52}$  to  $\text{An}_{34}$ ,

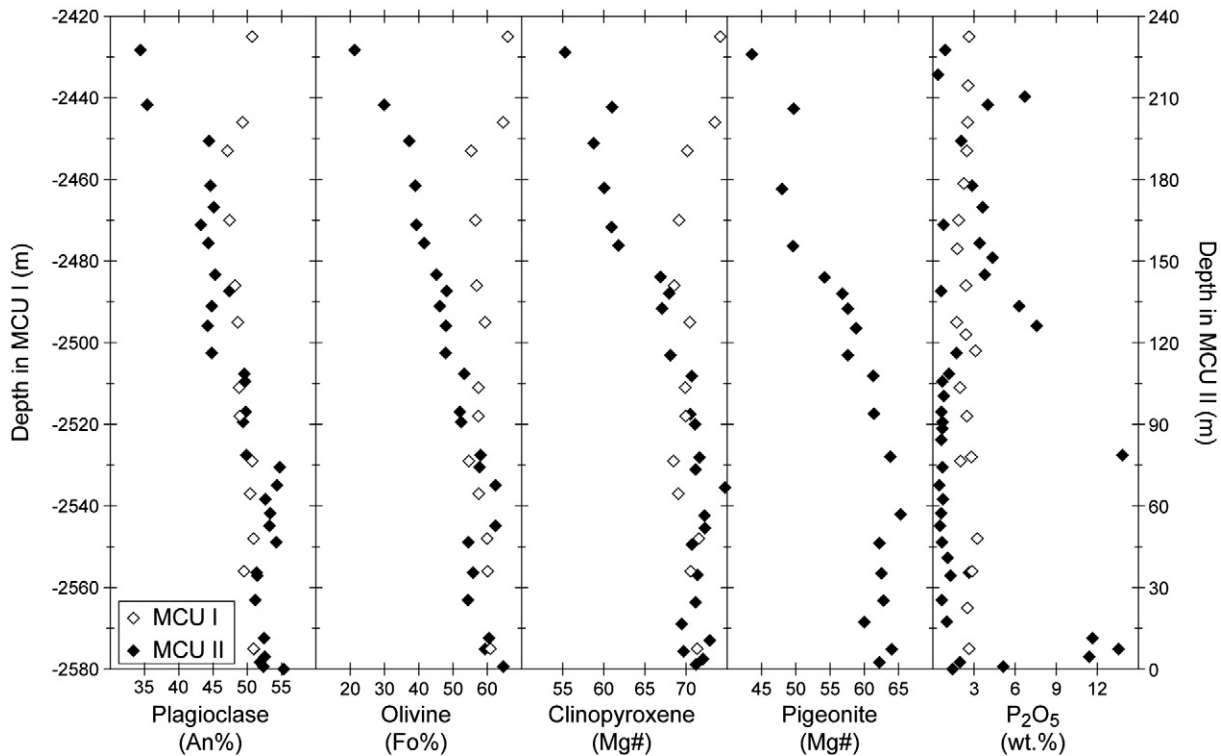


**Fig. 3.** Mineral and bulk-rock compositional variation with stratigraphy in Fe-Ti-P gabbro horizons of MCU I and MCU II. A. Plagioclase An-content. B. Olivine Fo-content. C. Clinopyroxene Mg#. D. Pigeonite Mg#. E. Bulk-rock  $P_2O_5$ -content.

olivine from  $Fo_{60}$  to  $Fo_{21}$ , clinopyroxene from  $Mg\#_{72}$  to  $Mg\#_{55}$  and pigeonite  $Mg\#_{65}$  to  $Mg\#_{44}$  (Supplementary Material 5; Fig. 3). No difference of mineral compositions is observed between leucocratic gabbros and melanocratic gabbros.

#### 4.3. Whole rock compositions and densities

Apatite-bearing gabbro of MCU I show a relatively restricted range of bulk compositions (e.g.  $SiO_2$ : 37.1–47.9 wt.%;  $FeO_t$ : 8.9–19.9 wt.%;  $MgO$ : 4.4–8.9 wt.%;  $P_2O_5$ : 1.7–3.2 wt.; Supplementary Material 6). When plotted as histograms, major element concentrations show a broadly symmetric distribution around a well-defined maximum in the mode (see the examples of  $FeO_t$  and  $P_2O_5$  in Fig. 4). Bulk-rock densities also show a relatively restricted range between 3.04 and 4.07  $g/cm^3$  (Fig. 4).

Rocks from the apatite-bearing gabbro horizon of MCU II show a larger range of bulk compositions (e.g.  $SiO_2$ : 3.7–50.4 wt.%;  $FeO_t$ : 8.0–55.7 wt.%;  $MgO$ : 2.5–10.7 wt.%;  $P_2O_5$ : 0.1–14.1 wt.%). When plotted as histograms, major element compositions are bimodal, with two well-defined maxima (see the examples of  $FeO_t$  and  $P_2O_5$  in Fig. 4). Intermediate compositions between those two maxima are very rare as illustrated by previously unpublished bulk-rock  $P_2O_5$  contents from various drill-cores analysed by the Soquem Inc. (Fig. 5). The bulk-rock density also shows a large range between 3.09 and 4.50  $g/cm^3$ , with a well defined bimodal distribution (Fig. 4; Charlier et al., 2011).

#### 5. Late-stage magmatic microstructures in the Layered Series

Magmatic microstructures resulting from late-stage reaction between silicate melt and primocrysts in cumulates of the Skaergaard intrusion have recently been investigated and were shown to give information on silicate liquid evolution during differentiation (Holness et al., 2011; Humphreys, 2011). Here we have investigated the distribution of these late-stage microstructures in the apatite-bearing

ferrogabbros collected for this study, and in an additional set of 250 cumulate rocks covering all the stratigraphic thickness of MCU I and MCU II (Namur et al., 2010).

Three types of late-stage microstructures, caused by reaction between liquid and primocrysts, have been identified in Sept Iles cumulate rocks.

- (1) Oxy-symplectites comprising intergrowths of orthopyroxene and magnetite that replace olivine grains in contact with magnetite. These symplectites are only observed in the structurally lower part of MCU I (po-C cumulates; Fig. 6A);
- (2) Orthopyroxene and plagioclase symplectites (the Type 2 reactive symplectite of Holness et al., 2011) that replace plagioclase primocrysts (Fig. 6B). This type of symplectite is generally closely associated with green/brown mica and is rooted on olivine grains. In Sept Iles, Type 2 symplectites are observed throughout MCU I, being more abundant in the lowest part (po-C cumulates). They are absent from MCU II (Fig. 6A);
- (3) Clinopyroxene-olivine-plagioclase ( $\pm$  amphibole,  $\pm$  biotite) symplectites (the Type 1 reactive symplectite of Holness et al., 2011) rooted on Fe-Ti oxide grains and replacing plagioclase primocrysts. Type 1 symplectites show a complicated stratigraphic distribution. They are almost absent from MCU I, except in a few samples at the top of the apatite-bearing gabbro unit (pomica-C) that have crystallized from a hybrid magma during a magma mixing event (Namur et al., 2010). They are, however, very common throughout MCU II, from the base of this megacyclic unit up to the appearance of cumulus apatite (pomi-C and pomic-C cumulates). In apatite-bearing gabbros of MCU II, Type 1 symplectites are generally absent (Fig. 6A).

The morphology of Type 1 symplectites evolves with stratigraphic position. In the lower and middle parts of MCU II, they are directly rooted on an oxide grain or are rooted to an intermediate biotite rim, itself rooted to the oxide grain (Fig. 6C). In some samples, the

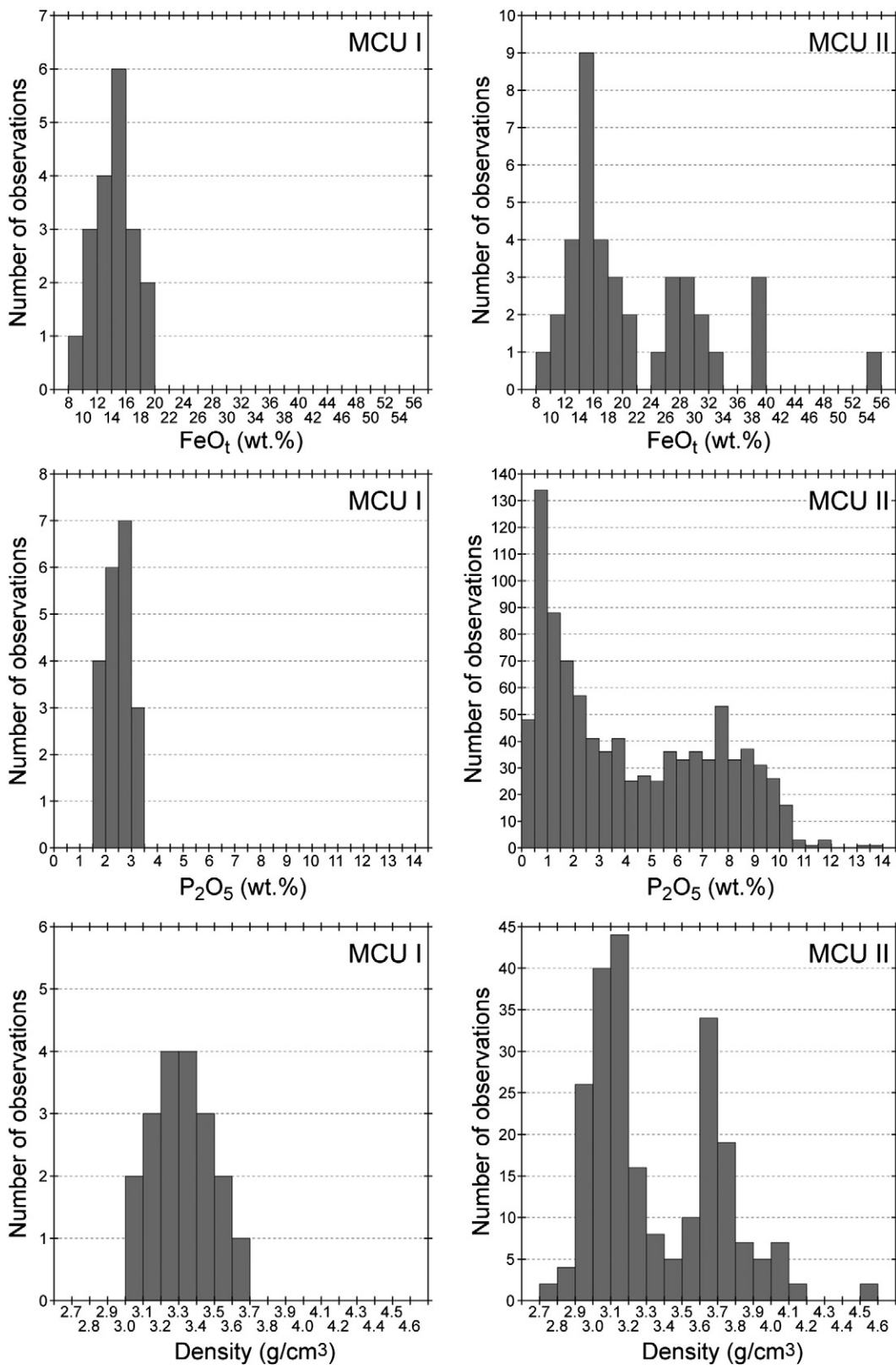
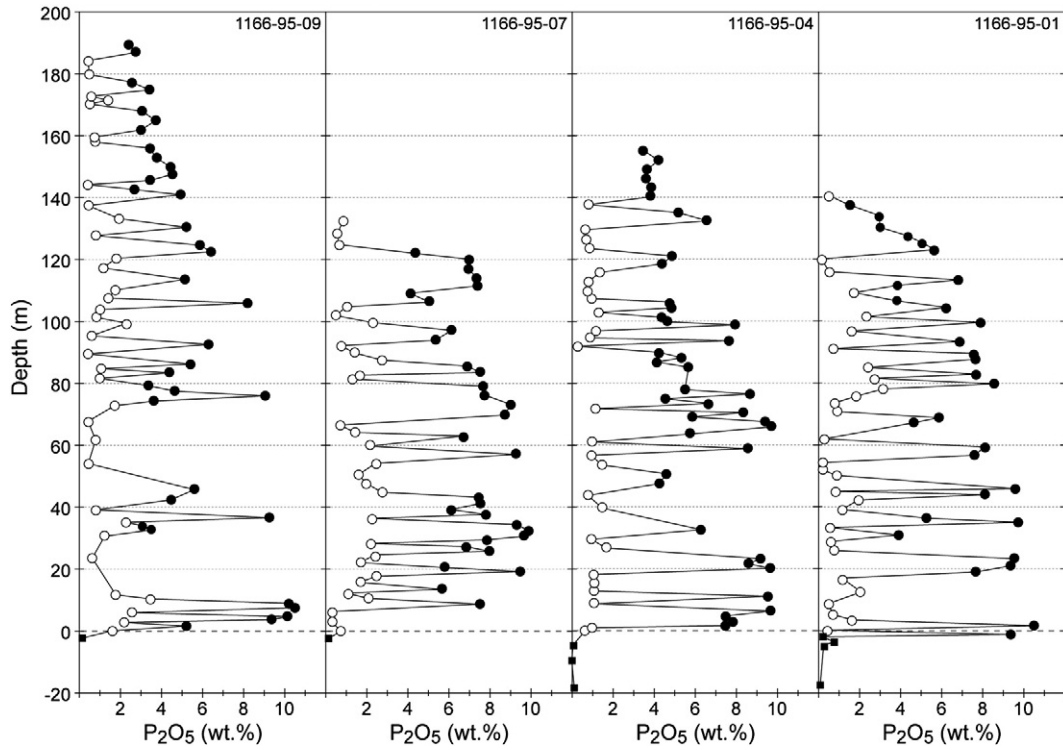


Fig. 4. Histograms for  $\text{FeO}_t$  (wt.%),  $\text{P}_2\text{O}_5$  (wt.%) and density ( $\text{g}/\text{cm}^3$ ) of Fe-Ti-P gabbros of MCU I and MCU II.

biotite rim may even form a symplectite with plagioclase (Fig. 6D). The morphology of Type 1 symplectites significantly changes 10 m below the appearance of cumulus apatite. In this 10 m-thick stratigraphic interval, Type 1 symplectites are still oxide-rooted and replace primocryst plagioclase, but symplectite colonies

are very coarse-grained and dominated by sub-equant, randomly oriented prisms of brown amphibole in addition to low aspect-ratio prisms of pyroxene, set in a single grain of plagioclase (Fig. 6E).

The rare symplectites found in the apatite-bearing gabbros of MCU II are found in those samples in which cm-scale Fe-Ti oxide- and



**Fig. 5.** Stratigraphic evolution of bulk-rock  $P_2O_5$  content in 4 representative drill-cores (out of a total of 30) kept by the Soquem Inc. They were drilled in 1995–1996 on the main-land, perpendicular to the layering, with an azimuth of  $325^\circ$ , along a 7 km traverse from the western part (1166-95-09) to the eastern part (1166-95-01) of the Sept Iles intrusion. Cores were split and individual samples are 0.32–13.2 m long (2.4 m on average). Phosphorous was measured using the gravimetric method by precipitation of magnesium ammonium phosphate hexahydrate. The “0 meter” reference level is defined as the stratigraphically lowest sample containing apatite (Namur et al., 2010). Black-squares represent samples from stratigraphic layers below the appearance of cumulus apatite. Black circles represent samples enriched in apatite (Fe-Ti-P-rich gabbros) and open circles represent samples depleted in apatite (Fe-Ti-P-poor gabbros). Note the small number of samples with intermediate  $P_2O_5$  content.

apatite-rich lenses occur within a highly leucocratic gabbro host (Fig. 6F). The boundary between the lenses and their host is marked by coarse-grained and well-developed symplectite colonies, rooted on the Fe–Ti oxide- and apatite-rich lens and growing into and replacing the leucogabbro (Fig. 6G).

## 6. Fractionation modeling

### 6.1. Methodology of calculation

We investigated the evolution of the Sept Iles melts using an incremental forward model of fractional crystallization. The model is based on a mass balance calculation between liquid and crystal mush (crystals + intercumulus liquid) for each major element oxide ( $SiO_2$ ,  $TiO_2$ ,  $Al_2O_3$ ,  $FeO$ ,  $Fe_2O_3$ ,  $MnO$ ,  $MgO$ ,  $CaO$ ,  $Na_2O$ ,  $K_2O$ ,  $P_2O_5$ ; Longhi, 1977; Thy et al., 2006; Toplis and Carroll, 1996):

$$c_{i,Liq}^0 = (1-z) * c_{i,Liq}^1 + z * \left[ \left( \sum_{j=1 \rightarrow n} X_j^i c_j^i \right) * X_{Sol}^{Mush} + c_{i,Liq}^0 X_{Liq}^{Mush} \right] \quad (1)$$

where  $z$  is the sequential increment of crystallization,  $c_{i,Liq}^1$  is the concentration of element  $i$  in the liquid at each step of fractionation,  $c_{i,Liq}^0$  is the concentration of element  $i$  in the liquid at the previous step of fractionation,  $c_j^i$  is the concentration of element  $i$  in the crystalline phase  $j$ ,  $X_j$  is the proportion of phase  $j$  in the cumulus assemblage,  $X_{Sol}^{Mush}$  is the bulk proportion of solid in the crystal + liquid mush and  $X_{Liq}^{Mush}$  is the proportion of intercumulus liquid in the crystal + liquid mush. The model was run for a proportion of remaining liquid decreasing from 1.0 to 0.4 with an increment ( $z$ ) of 0.01. The  $FeO/Fe_2O_3$  ratio of the liquid at each step of fractionation was calculated following the expression of Kress and

Carmichael (1991) using temperature estimates calculated from liquid composition following Eq. 15 of Putirka (2008).

For each step of fractionation, we used mineral compositions in equilibrium with the liquid of the previous step ( $c_{i,Liq}^0$ ). For plagioclase,  $CaO$ ,  $Na_2O$ ,  $SiO_2$  and  $Al_2O_3$  were calculated from Namur et al. (2012),  $FeO$  from Lundgaard and Tegner (2004) and  $K_2O$  from Thy et al. (2006). For olivine,  $FeO$ ,  $MgO$  and  $SiO_2$  were calculated from Toplis (2005),  $CaO$  from Libourel (1999) and  $MnO$  from Thy et al. (2006). For clinopyroxene,  $SiO_2$ ,  $FeO$ ,  $Fe_2O_3$ ,  $MgO$  and  $CaO$  were calculated from Toplis and Carroll (1996) and  $Al_2O_3$ ,  $MnO$  and  $Na_2O$  from Thy et al. (2006). For ilmenite and magnetite,  $FeO$ ,  $Fe_2O_3$  and  $TiO_2$  were calculated from Toplis and Carroll (1996), and  $MgO$  was regressed from the experimental data of Toplis and Carroll (1995).

For MCU I, we used the parental magma composition of the Sept Iles intrusion (Namur et al., 2010; Table 1; MCU I;  $F=1$ ) as the starting composition. The evolution of oxygen fugacity during crystallization of the Layered Series is poorly constrained, but it was estimated to be close to the FMQ (Fayalite–Magnetite–Quartz) buffer at the appearance of Fe–Ti oxide minerals (Namur et al., 2010). Here, we assumed the system is open to oxygen and buffered at FMQ throughout the considered interval of crystallization ( $F$ : 1.0–0.4). Because cotectic proportions are imposed on the model (see below), a small change of oxygen fugacity (FMQ + 1 to FMQ – 1) is not expected to have any significant effect on calculated liquid trends.

Here we improve on earlier fractionation models of iron-rich basaltic melts (Thy et al., 2006, 2009; Toplis and Carroll, 1996) by accounting for the effects of variable amounts of intercumulus liquid incorporated into the final, fully solidified rock. Following Namur and Charlier (2012) we assumed the cumulates retain 25% intercumulus liquid before the appearance of Fe–Ti oxides, and retain only 7% after oxide-saturation.

**Table 1**

Calculated liquid and mineral compositions.

MCU I											
	F = 1 Pl, OI	F = 0.9	F = 0.82 + Mt, Ilm	F = 0.8	F = 0.72 + Cpx	F = 0.7	F = 0.6	F = 0.52 + Apatite	F = 0.5	F = 0.43 Most evolved in MCU I	F = 0.4
SiO <sub>2</sub>	48.39	48.45	48.63	49.17	50.69	51.12	52.66	54.41	54.94	57.24	58.90
TiO <sub>2</sub>	2.84	3.14	3.46	3.42	3.24	3.19	2.82	2.45	2.42	2.31	2.28
Al <sub>2</sub> O <sub>3</sub>	14.45	13.58	12.62	12.40	12.01	11.89	11.75	11.63	11.55	11.28	11.32
FeO <sub>t</sub>	14.82	15.70	16.65	16.50	15.91	15.82	15.03	14.20	14.12	13.74	13.68
MnO	0.24	0.26	0.27	0.28	0.30	0.31	0.33	0.36	0.37	0.40	0.42
MgO	5.45	5.12	4.85	4.82	4.57	4.54	4.24	3.95	3.77	3.15	2.96
CaO	9.69	9.52	9.18	9.03	8.71	8.46	8.12	7.54	7.34	6.29	4.73
Na <sub>2</sub> O	2.77	2.76	2.75	2.73	2.74	2.75	2.88	2.99	3.01	3.07	3.11
K <sub>2</sub> O	0.78	0.84	0.90	0.94	1.03	1.10	1.21	1.37	1.42	1.63	1.74
P <sub>2</sub> O <sub>5</sub>	0.57	0.63	0.69	0.71	0.80	0.82	0.96	1.10	1.06	0.91	0.86
Mg#	0.396	0.368	0.343	0.342	0.339	0.338	0.335	0.331	0.322	0.290	0.278
Plagioclase An	70.5	66.5	62.4	62.1	60.3	59.9	56.6	51.8	51.2	47.1	40.0
Olivine Fo	71.6	69.1	66.8	66.6	66.4	66.3	66.1	64.7	62.7	57.2	53.2
Cpx Mg#	—	—	—	—	74.2	74.0	73.4	72.5	71.5	69.3	66.3

MCU II										
	F = 1 Pl, OI, Mt, Ilm, Cpx	F = 0.9	F = 0.8	F = 0.7	F = 0.64 + Apatite	F = 0.6	F = 0.5	F = 0.44 Most evolved in MCU II		F = 0.4
SiO <sub>2</sub>	51.81	53.12	54.98	56.89	58.64	59.67	63.11	66.42		68.77
TiO <sub>2</sub>	2.68	2.57	2.39	2.20	2.01	1.99	1.91	0.19		1.93
Al <sub>2</sub> O <sub>3</sub>	13.51	13.13	12.63	12.18	11.80	11.57	10.88	14.66		10.05
FeO <sub>t</sub>	14.55	14.11	13.45	12.74	12.06	11.90	11.19	8.95		10.00
MnO	0.29	0.31	0.33	0.36	0.38	0.39	0.43	0.48		0.50
MgO	4.39	4.20	3.92	3.63	3.37	3.05	2.08	1.27		1.10
CaO	8.15	7.64	6.91	6.18	5.53	5.12	3.81	1.65		0.71
Na <sub>2</sub> O	2.88	3.00	3.17	3.32	3.45	3.49	3.62	3.48		3.73
K <sub>2</sub> O	1.05	1.18	1.35	1.54	1.70	1.81	2.15	2.31		2.67
P <sub>2</sub> O <sub>5</sub>	0.68	0.75	0.86	0.97	1.07	1.01	0.81	0.59		0.54
Mg#	0.351	0.346	0.342	0.337	0.332	0.314	0.249	0.208		0.163
Plagioclase An	63.2	61.4	58.5	54.8	51.8	50.0	43.4	34.1		21.7
Olivine Fo	68.1	66.4	65.2	63.5	61.4	51.7	34.5	29.7		24.6
Cpx Mg#	75.6	74.5	72.4	71.5	68.2	57.4	43.6	40.6		36.7

Following the sequence of crystallization and mineral compositions described in Namur et al. (2010), the model starts with the crystallization of plagioclase and olivine (po-C) in cotectic proportions (Pl/OI: 76/24; Namur et al., 2011a, 2011b) from the parental magma (MCU I; F = 1; Table 1) and Fe-Ti oxides (pomi-C), clinopyroxene (pomic-C) and apatite (pomica-C) are added to the liquidus assemblage when the calculated plagioclase composition reaches An<sub>63</sub>, An<sub>60</sub> and An<sub>52</sub>, respectively. Mineral cotectic proportions in the Sept Iles gabbros are unknown. We varied them, by trial and error, until the model (Eq. (1)) reproduces the plagioclase compositional trend observed in MCU I (Namur et al., 2010). The resulting cotectic proportions are: pomi-C: Pl/OI/Mt/Ilm: 58:20:16:6; pomic-C: Pl/OI/Mt/Ilm/Cpx: 40:5:16:6:33; pomica-C: Pl/OI/Mt/Ilm/Cpx/Ap: 45:18:8:4:20:5. These are not significantly different to the average mineral modes observed in the Layered Series (Table 2; Namur et al., 2010).

For MCU II, the model starts with the crystallization of pomic-C cumulates and apatite is added when the plagioclase composition reached An<sub>52</sub>. As detailed below, the parent magma composition was calculated by mixing the residual magma of MCU I with the parent magma of the intrusion.

## 6.2. Calculated mineral compositions: A test of the model

Comparison between calculated mineral compositions and those observed in cumulate rocks of MCU I provides a test for the reliability of our fractionation model in estimating the Sept Iles liquid lines of descent, assuming that reproduction of observed compositions is only possible if calculated liquids are close to the actual Sept Iles liquid line of descent. The good match between calculated plagioclase compositions and those observed in MCU I (Fig. 7A) is not relevant because cotectic proportions of cumulus phases were selected to reproduce the plagioclase compositional trend of MCU I. However, the very good correlation observed between calculated olivine (Fo) and clinopyroxene (Mg#) compositions with those observed in rocks from MCU I, illustrated in Figs 7B and 7C, demonstrates the reliability of the forward model in predicting accurate liquid lines of descent.

## 6.3. Liquid compositions

In the interval of crystallization from 0 to 60% (F = 1–0.4), the calculated residual liquid of MCU I evolves from a tholeiitic basalt (SiO<sub>2</sub>:

**Table 2**

Cotectic proportions used in the model of fractional crystallization and comparison with modal proportions in the Layered Series.

Cumulus assemblage	Cotectic proportions used in fractionation modeling						Average mineral modes in the Layered Series					
	Plag	Olivine	Mgt	Ilm	Cpx	Ap	Plag	Olivine	Mgt	Ilm	Cpx	Ap
po-C	76	24	—	—	—	—	71	29	—	—	—	—
pomi-C	58	20	16	6	—	—	55	23	15	7	—	—
pomic-C	40	5	16	6	33	—	42	7	13	7	31	—
pomica-C	45	18	8	4	20	5	48	16	8	6	17	5

Plag: plagioclase; Mgt: magnetite; Ilm: ilmenite; Cpx: clinopyroxene; Ap: apatite.

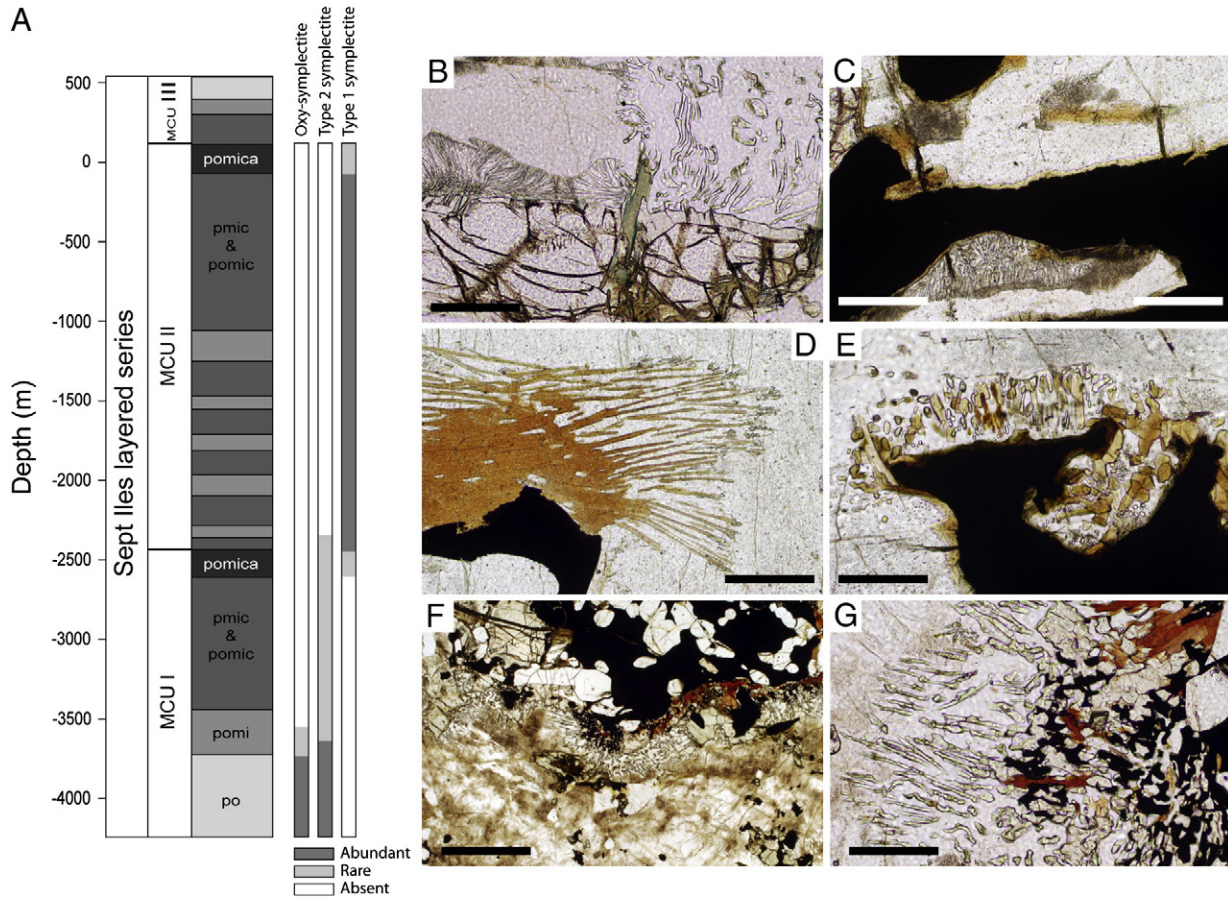


**Fig. 6.** Stratigraphic column of the Sept Iles intrusion showing the distribution of rock-types (troctolites: po-C; Fe-Ti oxide-troctolites: pomi-C; gabbros: pomic-C and pmic-C; apatite-bearing gabbros: pomica-C; p = plagioclase, o = olivine, m = magnetite; i = ilmenite; a = apatite; -C = cumulus; classification following Irvine, 1982). A. Stratigraphic distribution of the symplectites (oxy-symplectites, Type 1 and Type 2 reactive symplectites; Holness et al., 2011) observed in Sept Iles cumulate rocks from MCU I and MCU II. B. Type 2 symplectite of orthopyroxene and plagioclase growing from primocryst olivine and replacing primocryst plagioclase. The olivine is separated from the symplectite by a rim of orthopyroxene. Note the green/brown mica associated with the olivine-rooted symplectite. Sample DC-9-2111.5; po-C unit, MCU I; transmitted light. C. Type 1 oxide-rooted symplectite of pyroxene and plagioclase replacing a plagioclase primocryst. Note the biotite rim separating the symplectite from the oxide root. The grain size of the lamellae decreases from the oxide, denoting the growth direction was into the primocryst plagioclase grain. Sample DC-8-476; pomi-C unit, MCU II; transmitted light. D. Type 1 oxide-rooted symplectite dominated by plagioclase and biotite, with only a thin outer zone containing pyroxene. Sample DC-8-570; pomi-C unit; MCU II; transmitted light. E. Type 1 oxide-rooted symplectite dominated by amphibole, with plagioclase and minor pyroxene and biotite, replacing a primocryst plagioclase grain. Note the dusting of the primocryst plagioclase with “exsolved” pyroxene. Sample ON-07-155; pmic-C unit; MCU II; transmitted light. F–G. Symplectite colonies of clinopyroxene and plagioclase (with an inner zone of oxides, pyroxene, biotite and plagioclase) growing from a small (cm-scale) Fe-Ti oxide- and apatite-rich lens (with some feldspar) into the enclosing leucogabbro host. Sample s9-106.3; pomica-C unit; MCU II; transmitted light. Scale bar is 200  $\mu\text{m}$ , except in F (1 mm).

48.8 wt.%; Mg#: 0.396; Table 1) to a moderately evolved trachy-andesite ( $\text{SiO}_2$ : 58.9 wt.%; Mg#: 0.278; Fig. 8). The most evolved liquid of MCU I, in equilibrium with plagioclase  $\text{An}_{47}$ , is a trachy-andesite ( $\text{SiO}_2$ : 57.2 wt.%; Mg#: 0.290;  $F=0.43$ ; MCU I; Table 1).

The most primitive plagioclase of MCU II is  $\text{An}_{63}$  (Namur et al., 2010). We have thus evaluated the parent magma composition of MCU II by mixing the most evolved residual liquid of MCU I ( $\text{SiO}_2$ : 57.2 wt.%;  $\text{An}_{47}$ ;  $F=0.43$ ; MCU I; Table 1) with the parental magma of MCU I ( $\text{SiO}_2$ : 48.8 wt.%;  $\text{An}_{67}$ ;  $F=1$ ; MCU I; Table 1) by successive fractions of 0.5 wt.%. The equilibrium plagioclase composition was calculated for each hybrid liquid, and the parent magma to MCU II was considered to be in equilibrium with  $\text{An}_{63}$  (Fig. 9). This liquid results from mixing between 30 vol.% of residual liquid from MCU I and 70% of undifferentiated magma.

The parental magma of MCU II was found to be an evolved tholeiitic basalt (51.5 wt.%  $\text{SiO}_2$ ; Mg#: 0.368;  $F=1$ ; MCU II; Table 1). In the interval of crystallization from 0 to 60% ( $F=1$ –0.4), the residual liquid of MCU II evolves towards a dacite ( $\text{SiO}_2$ : 68.8 wt.%; Mg#: 0.163;  $F=0.4$ ; MCU II; Table 1; Fig. 8). The most evolved liquid of

MCU II, in equilibrium with plagioclase  $\text{An}_{34}$ , is a dacite ( $\text{SiO}_2$ : 66.5 wt.%; Mg#: 0.208;  $F=0.44$ ; MCU II; Table 1). This liquid is compositionally similar to the most primitive enclave-free granites observed in the Upper Series ( $\text{SiO}_2$ : 65.2 wt.%; Mg#: 0.142) and interpreted as residual liquids from MCU II (Namur et al., 2011a).

## 7. Discussions

### 7.1. Effect of magma mixing on Sept Iles liquid lines of descent

Magma mixing is an important process in the evolution of the Sept Iles intrusion. After the crystallization of MCU I from a single batch of magma, the chamber was replenished by the arrival of many new batches of magma, expanding the magma chamber and forming MCU II and MCU III (Namur et al., 2010). During differentiation of the magma batch that formed MCU I, most major elements evolve along a curved (e.g.  $\text{CaO}$ ,  $\text{MgO}$ ,  $\text{Na}_2\text{O}$ ), a half-bell shaped (e.g.  $\text{FeO}$ ,  $\text{TiO}_2$ ,  $\text{Al}_2\text{O}_3$ ) or bell-shaped ( $\text{P}_2\text{O}_5$ ) liquid line of descent, rather than following a linear liquid line of descent (Fig. 8). The overall effect of this non-linear shape is that magma mixing produced liquid

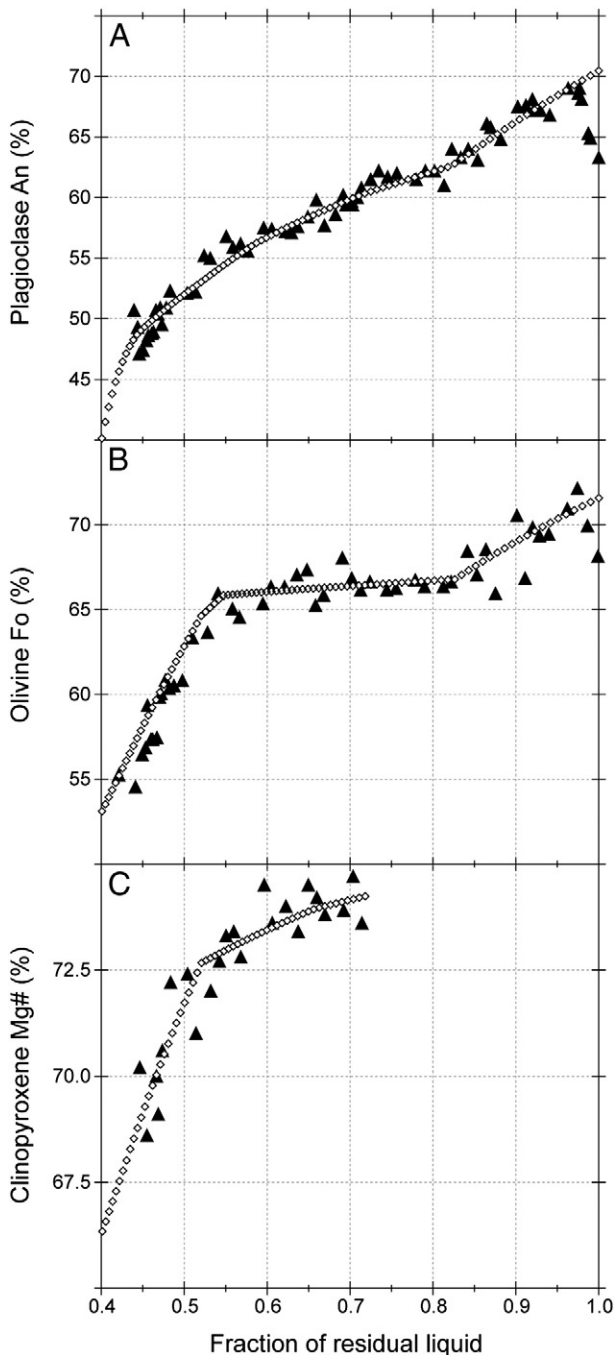


**Fig. 7.** Comparison of MCU I mineral compositions calculated using the incremental fractionation model and mineral compositions measured by electron microprobe (Namur et al., 2010). A. Plagioclase An-content. B. Olivine Fo-content. C. Clinopyroxene Mg#. The proportion of residual liquid in the magma chamber at the stratigraphic height of each natural sample is calculated following Namur and Charlier (2012).

compositions plotting away from the differentiation path of MCU I. As a consequence, the parent magma of MCU II was an evolved hybrid composition that bears little relationship with the magma from which MCU I crystallized. The absence of primitive troctolites in MCU II, together with fractionation of evolved Fe-Ti oxide- and cpx-bearing ferrogabbros, means that the MCU II magma was driven towards strong SiO<sub>2</sub>-enrichment and FeO<sub>t</sub>-depletion. Liquid compositions reached at the top of MCU II are significantly more evolved than those at the top of MCU I. The timing of mineral saturation (value of F at the appearance of a new liquidus phase) is also different in MCU I

compared to MCU II (e.g. apatite; Fig. 8; Tollari et al., 2006). These differences produced contrasted cumulate sequences in MCU I and MCU II and eventually affected magma chamber processes during crystallization.

There are two main differences between the mineralogical and geochemical characteristics of apatite-bearing rocks in the Sept Iles intrusion: (1) rocks from MCU II are characterized by a significant modal proportion of pigeonite, a phase which is not present in MCU I (Fig. 2); and (2) rocks from MCU II show a large range of bulk compositions (bimodal for most elements), while rocks from MCU I have a highly restricted, unimodal range of compositions (Fig. 4). In the following, we will show that these differences may be explained by the effects of hybridization during magma mixing in MCU II.

### 7.2. Stability of pigeonite

Pigeonite is a moderately abundant cumulus phase in MCU II, appearing simultaneously with apatite and well after clinopyroxene and Fe-Ti oxide, but is absent in MCU I. This is presumably related to compositional differences between the respective parental liquids. A review of 23 experimental studies by Veksler (2009) has shown that the assemblage plagioclase + olivine + clinopyroxene + pigeonite + liquid, as observed in rocks from MCU II, does not provide narrow constraints on liquid composition (e.g. SiO<sub>2</sub>: 41.7–65.7; FeO<sub>t</sub>: 7.6–29.9; CaO: 4.1–13.1), as expected for a 5 phase assemblage (Grove and Juster, 1989). Experimental studies have shown the critical role of P<sub>2</sub>O<sub>5</sub> and alkalis (Na<sub>2</sub>O and K<sub>2</sub>O) in stabilizing a low-Ca pyroxene in the liquidus assemblage (Charlier and Grove, 2012; Grove and Juster, 1989; Tollari et al., 2006; Toplis et al., 1994). Experiments by Toplis et al. (1994), carried out under constant pressure (1-atm) and temperature (1072 °C), show that the stability field of pigeonite is enhanced by increasing the liquid P<sub>2</sub>O<sub>5</sub> content. Furthermore, for relatively constant liquid P<sub>2</sub>O<sub>5</sub> contents (0–1.5 wt.%), pigeonite saturation will occur in the most SiO<sub>2</sub>- and alkali-rich and MgO-poor melts, in good agreement with the experimental results of Grove and Juster (1989) and Shi (1993).

Pigeonite appears in MCU II simultaneously with apatite. A comparison of liquid composition at the point of apatite saturation in MCU I and MCU II should therefore allow us to determine why pigeonite is a cumulus phase in MCU II while it is absent in MCU I. Saturation of apatite occurs both in MCU I and MCU II when the liquid reaches ca. 1.1 wt.% P<sub>2</sub>O<sub>5</sub> (Fig. 8). At apatite saturation, the liquid from MCU II is enriched in SiO<sub>2</sub> and alkalis and contrastingly depleted in MgO compared to the liquid from MCU I, therefore favoring pigeonite stability in MCU II. This is confirmed by plotting MCU I and MCU II liquid lines of descent from plagioclase onto the pseudoternary plane olivine, clinopyroxene (Cpx) and quartz (Qtz; Fig. 10), following the normalization procedure of Grove et al. (1982). As shown in Fig. 10, liquid lines of descent characterized by the longest fractionation interval with SiO<sub>2</sub>-enrichment are the most likely to encounter the pigeonite stability field. The MCU I liquid line of descent is characterized by an early FeO<sub>t</sub>-enrichment followed by a trend of SiO<sub>2</sub> enrichment for less than 30% of fractionation. MCU I liquids will therefore be located in the Cpx-rich and Qtz-poor of the pseudoternary plane, and are unlikely to encounter the pigeonite field. In contrast, the MCU II liquid line of descent is characterized by a continuous FeO<sub>t</sub>-decrease and SiO<sub>2</sub>-enrichment. Liquids thus evolve towards the Qtz pole and are therefore more likely to encounter the pigeonite field during their evolution.

### 7.3. Homogeneous melt vs immiscibility

Immiscibility between Fe-rich and Si-rich liquids has been identified in evolved ferrogabbros of various layered intrusions, such as Skaergaard (Holness et al., 2011; Humphreys, 2011; Jakobsen et al., 2005, 2011; Mc Birney, 1975), Sept Iles (Charlier et al., 2011), Duluth

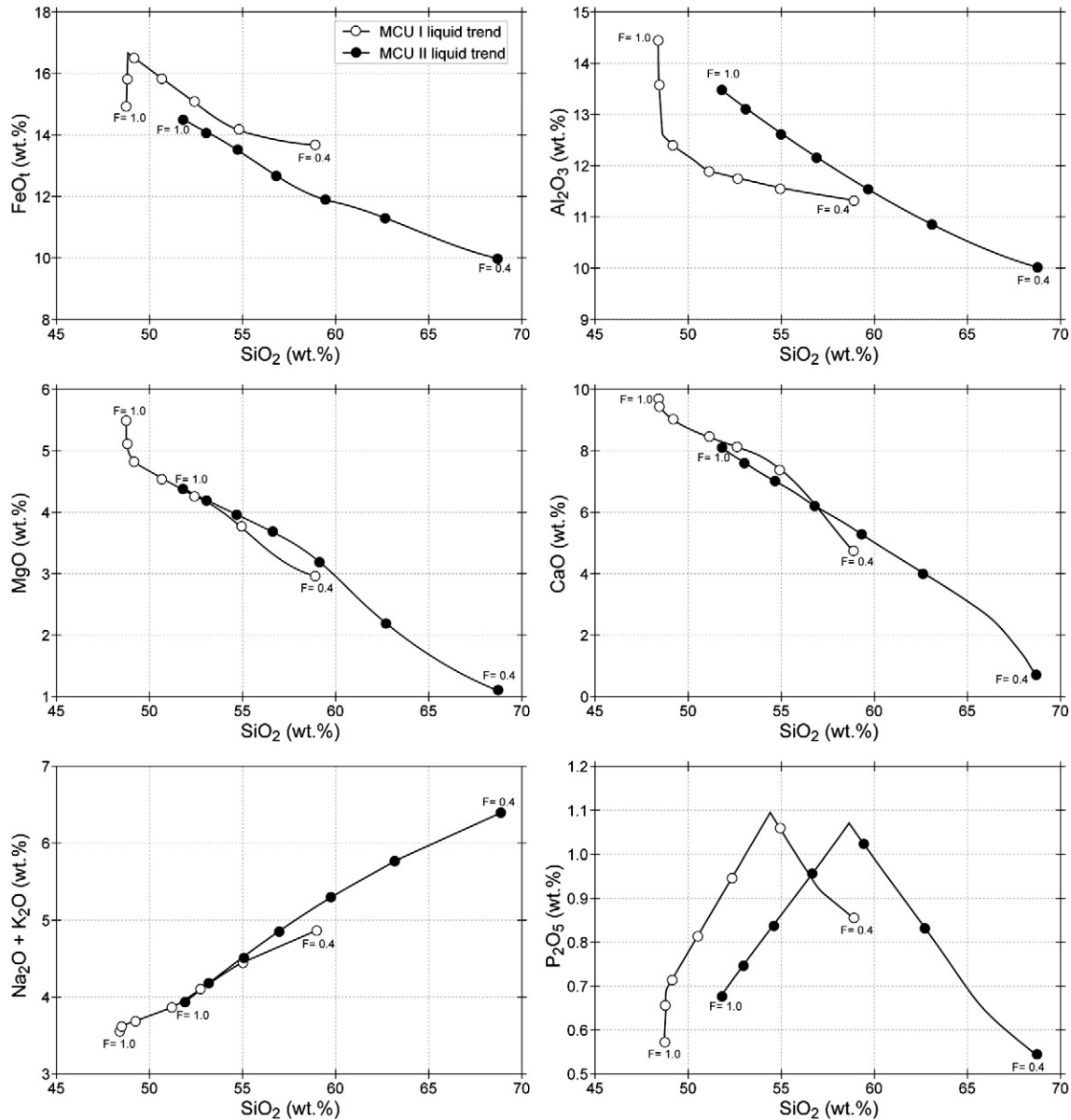


**Fig. 8.** Calculated MCU I (open circles) and MCU II (filled circles) liquid lines of descent for selected major elements (wt.%) vs  $\text{SiO}_2$  (wt.%). F = fraction of residual liquid. Distance between each circle corresponds to 10% of fractionation.

(Ripley et al., 1998) and Bushveld (Van Tongeren and Mathez, 2012). Detailed geochemical studies of bulk-rocks and melt inclusions have shown that the two immiscible liquids may undergo large-scale segregation in layered intrusions of the size of Sept Iles and Bushveld (Charlier et al., 2011; Van Tongeren and Mathez, 2012), while such large-scale segregation does not seem to occur in smaller (e.g. 10 km) magma chambers (Jakobsen et al., 2011).

Large-scale segregation of immiscible liquids results in the crystallization of two types of ferrogabbros: a leucogabbro that crystallizes from the Si-rich melt and a melanogabbro that crystallizes from the Fe-rich melt (Charlier et al., 2011; Van Tongeren and Mathez, 2012). Silicate liquid immiscibility together with large-scale separation of the immiscible melts therefore provides an explanation for the bimodality observed in bulk-rock compositions of apatite-bearing cumulates of MCU II (Charlier et al., 2011). In contrast, the unimodal distribution of MCU I bulk-rock compositions is consistent with crystallization from a homogeneous silicate melt, i.e. immiscibility did not occur during the crystallization of MCU I.

#### 7.4. Onset of silicate liquid immiscibility

Iron is known to expand the immiscibility field (Roedder, 1951, 1978; Visser and Koster van Groos, 1979a) and it is generally thought that extreme liquid FeO<sub>t</sub>-enrichment is the key parameter in controlling whether a silicate liquid will unmix or not (Dixon and Rutherford, 1979; Martin and Kushiro, 1991; McBirney and Nakamura, 1973; McBirney and Naslund, 1990; Naslund, 1983; Philpotts and Doyle, 1983). Nevertheless, experiments by Charlier and Grove (2012) have shown that unmixing can develop from  $\text{SiO}_2$ -rich and relatively FeO<sub>t</sub>-poor silicate liquids. Other elements such as TiO<sub>2</sub>, P<sub>2</sub>O<sub>5</sub> and alkalis ( $\text{Na}_2\text{O} + \text{K}_2\text{O}$ ) either enlarge the two-liquid field or decrease the melt liquidus temperature, favoring liquid–liquid unmixing (Bogaerts and Schmidt, 2006; Charlier and Grove, 2012; Visser and Koster van Groos, 1979b; Watson, 1976). In contrast, CaO and MgO increase the melt liquidus temperature and depress the two-liquid field (Bogaerts and Schmidt, 2006; Hoover and Irvine, 1978). Increasing the concentration of these elements in the melt stabilizes a single liquid phase.

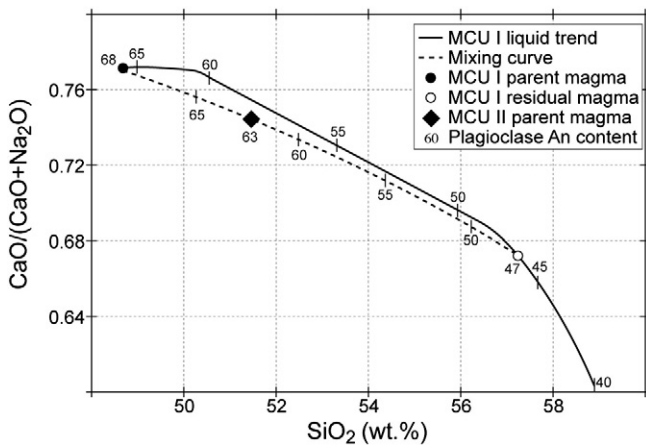


**Fig. 9.**  $\text{CaO}/(\text{CaO} + \text{Na}_2\text{O})$  vs.  $\text{SiO}_2$  (wt.%) diagram showing calculated liquid line of descent and equilibrium plagioclase compositions of MCU I. The dashed curve corresponds to a mixing curve between the parent magma of MCU I and the most evolved residual liquid of MCU I (See Table 1). Calculated plagioclase compositions along the mixing curve are indicated. The parent magma composition of MCU II corresponds to the liquid along the mixing curve in equilibrium with plagioclase  $\text{An}_{63}$ .

Comparison between the liquid lines of descent of MCU I and MCU II is here used to explain why immiscibility developed in MCU II but did not in MCU I. Experiments by Charlier and Grove (2012) have been performed on natural basalts relevant to various ferrobasaltic volcanic provinces and layered intrusions, including the Sept Iles intrusion. These experiments take into account the effect of both major (e.g.  $\text{SiO}_2$ ,  $\text{FeO}$ ,  $\text{CaO}$ ,  $\text{MgO}$ ) and minor (e.g. alkalis,  $\text{P}_2\text{O}_5$ ) elements to define the compositional space where immiscibility develops. While many elements contribute to whether a silicate liquid will unmix or not, Charlier and Grove (2012) have shown that in the simple compositional space  $\text{SiO}_2/3 - \text{CaO} - \text{Al}_2\text{O}_3$ , systems high in  $\text{SiO}_2$  and  $\text{Al}_2\text{O}_3$  will produce liquid–liquid unmixing, while systems enriched in  $\text{CaO}$  and relatively poor in  $\text{SiO}_2$  and  $\text{Al}_2\text{O}_3$  will contain a single liquid phase (Fig. 11). The position of the binodal in Fig. 11 was determined using 30 experimental

immiscible liquids. When calculated liquid lines of descent for MCU I and MCU II are plotted, it is apparent that liquids from MCU I do not cross the binodal and immiscibility does not develop. In contrast, liquids from MCU II cross the binodal soon after the saturation of apatite and liquid–liquid immiscibility is likely to have occurred during crystallisation of MCU II.

### 7.5. Formation of Fe–Ti–P gabbros and implications for the Bushveld Complex

A consideration of the chemical composition of the liquids from which MCU I and MCU II crystallized shows that immiscibility is very likely to have developed at the top of MCU II, while MCU I crystallized entirely from a homogeneous melt. This suggestion is supported by the observed distribution of symplectites in cumulate rocks of the Layered Series (Fig. 5). In the Skaergaard intrusion, oxy-symplectites and Type 2 reactive symplectites are thought to record reaction between cumulus phases and a single homogenous intercumulus melt (Holness et al., 2011), while oxide-rooted Type 1 reactive symplectites are interpreted as a result of reaction between cumulus phases and an Fe-rich immiscible melt, consequent to the loss of the buoyant conjugate Si-rich immiscible liquid from the mushy layer (Holness et al., 2011). Given the similar cumulus assemblages and parental liquids of the Skaergaard and Sept Iles intrusions, we suggest a similar interpretation of the symplectites in Sept Iles. In Sept Iles, oxy-symplectites and type 2 reactive symplectites are only observed in MCU I, confirming that the intercumulus melt that crystallized in the pore space of MCU I rocks did not enter the two-liquid immiscibility field. In contrast, the commonly observed oxide-rooted Type 1 symplectites in MCU II indicate that the intercumulus melt of this megacyclic unit split into two immiscible liquids at the end of its differentiation path, in agreement with our calculated MCU II liquid line of descent.

Crystallization of a homogeneous melt in MCU I produced rocks that are unimodal in terms of mineral modes and bulk-rock compositions. In contrast, immiscibility in MCU II, together with the small cooling rate of a large magma chamber, allowed coalescence of immiscible globules (Martin and Kushiro, 1991) and efficient gravitational segregation of the two liquids. Liquid–liquid segregation resulted in crystallization of ferrogabbros with various modal proportions but similar mineral compositions, explaining the bimodal bulk-rock compositions observed in the apatite-bearing horizon of MCU II. The alternation of Fe–Ti–P rich gabbros and Fe–Ti–P poor gabbros at the 5–20 m scale is explained by immiscibility not affecting the entire mass of residual liquid in the magma chamber, but occurring repetitively in a basal boundary layer unaffected by convection at the interface between the cumulate pile and the main magma body (Charlier et al., 2011; Jaupart et al., 1984). Thirty 100 m deep drill-cores extracted along a 7 km traverse in ferrogabbros of MCU II attest to the lateral continuity of the melanocratic and leucocratic layers.

The Upper Zone of the Bushveld complex crystallized from a hybrid evolved tholeiitic basalt (Kruger et al., 1987; Tegner et al., 2006; VanTongeren et al., 2010) with a sequence of crystallization similar to those observed in Skaergaard and Sept Iles (Eales and Cawthorn, 1996; McBirney, 1996; Namur et al., 2010; Tegner et al., 2006; VanTongeren et al., 2010). The upper part of this unit (Upper Zone C) is characterized by the presence of alternating horizons of Fe–Ti–P-rich and Fe–Ti–P-poor gabbros (Tegner et al., 2006; VanTongeren and Mathez, 2012), though their origin is not well understood (Cawthorn and Ashwal, 2009; Tegner et al., 2006). We suggest that they might result from a process of large-scale silicate liquid immiscibility, in a similar manner to that we have suggested for Sept Iles. Using a forward model similar to that used in this paper, Tegner et al. (2006) have shown that the liquid of the Bushveld Upper Zone evolves with differentiation from basalt to dacite. The Bushveld Upper Zone liquid line of descent intersects the two-liquid field defined by Charlier and

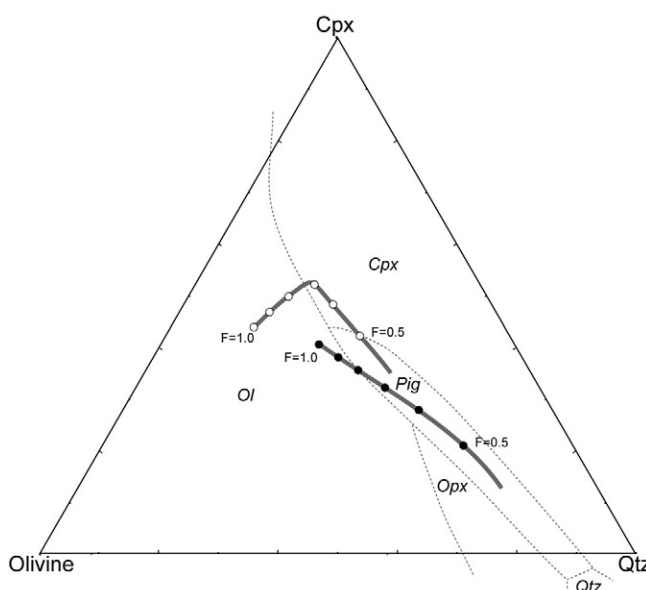


**Fig. 10.** Liquids line of descent of MCU I (open circles) and MCU II (filled circles) projected from plagioclase onto the pseudoternary clinopyroxene (Cpx)–olivine–quartz (Qtz) following the procedure of Grove et al. (1982). Mineral stability field boundaries after Grove and Baker (1984). F: Fraction of residual liquid. Distance between each circle corresponds to 10% of fractionation.

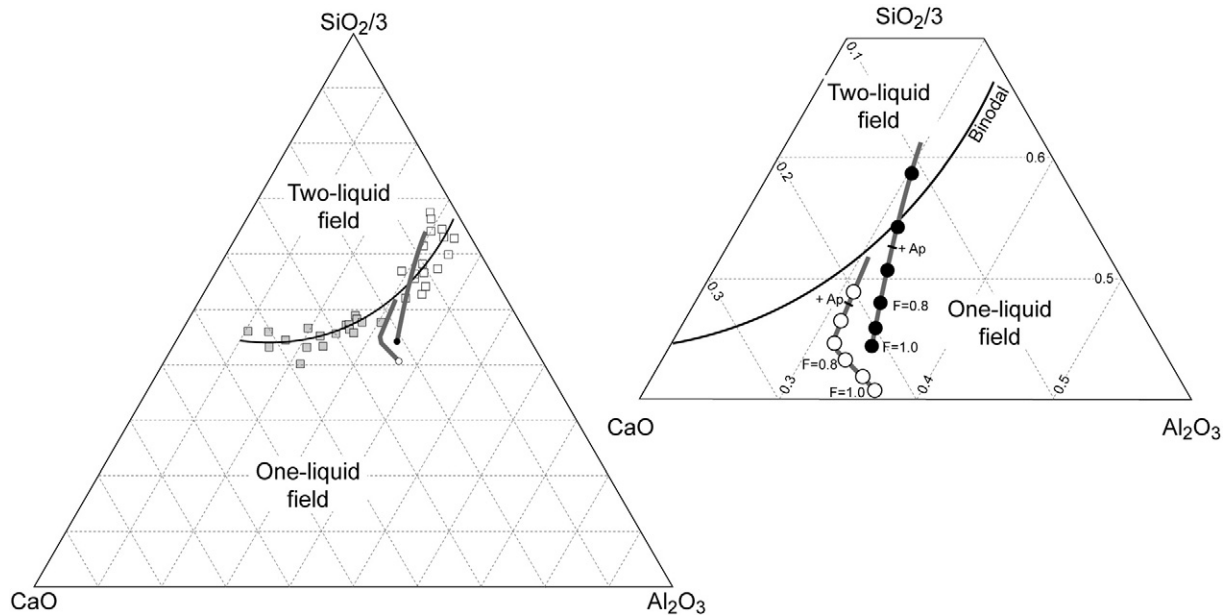


**Fig. 11.** a. Representation of MCU I (open circles) and MCU II (filled circles) liquid lines of descent in the ternary diagram  $\text{SiO}_2/3\text{--CaO--Al}_2\text{O}_3$ . One-liquid field, two-liquid field and the position of the binodal have been determined using the composition of 30 immiscible melts from Charlier and Grove (2012). b. Close-up view of the liquid lines of descent and the binodal. F: Fraction of residual liquid. Ap: Apatite. Distance between each circle corresponds to 10% of fractionation.

Grove (2012) on the  $\text{SiO}_2/3\text{--CaO--Al}_2\text{O}_3$  ternary diagram (Fig. 12), consistent with the onset of liquid immiscibility. The large size of the intrusion and the consequent slow cooling rate (Irvine, 1970) will increase the efficiency of coalescence and gravitationally-driven separation of immiscible globules. Immiscibility in the upper part of the Bushveld complex might therefore adequately explain the formation of cm-dm thick Fe-Ti-P-rich gabbros layers alternating with m-thick Fe-Ti-P-poor gabbros layers (Tegner et al., 2006; Van Tongeren and Mathez, 2012).

## 8. Conclusions

The formation of ferrogabbros from evolved tholeiitic basalts can result either from the crystallization of a homogeneous silicate melt, or from the solidification of immiscible Fe-rich and Si-rich melts. Whether tholeiitic liquid lines of descent will enter the two-liquid field or stay within the one-liquid field depends on minor differences of liquid composition as illustrated by the ternary  $\text{CaO--Al}_2\text{O}_3\text{--SiO}_2$  diagram of Charlier and Grove (2012).

The liquid line of descent for Megacyclic Unit I (MCU I) of the Sept Iles layered did not enter the two-liquid field. In contrast, residual liquids from MCU II underwent unmixing with the formation of a conjugate pair of a Si-rich liquid and an Fe-rich liquid. The contrasted differentiation paths experienced by these different components of the Sept Iles intrusion had major implications for mineral proportions and bulk-rock compositions of the resultant cumulate rocks. In MCU I, crystallization from a homogeneous melt produced leucocratic to moderately melanocratic ferrogabbros with mineral proportions close to theoretical cotectic proportions of an apatite-saturated evolved tholeiitic melt. In MCU II silicate liquid immiscibility together with the slow cooling rate of the intrusion allowed the efficient segregation of the two immiscible liquids, producing two contrasted types of ferrogabbros: (1) highly melanocratic ferrogabbros dominated Fe-Ti oxides, pyroxenes and olivine, with minor plagioclase, and (2) leucocratic ferrogabbros dominated by plagioclase. The contrasted liquid lines of descent between MCU I and MCU II also resulted in differences in the pigeonite mode, with abundant pigeonite in MCU II but none in MCU I.

Our calculated liquid line of descent of MCU II is remarkably similar to that estimated for the Upper Zone of the Bushveld Intrusion. We therefore suggest that immiscibility might have played a significant role in the formation of the ferrogabbros occurring at the top of the Bushveld. Given the large size of the intrusion and the likely very slow cooling rate, we might expect efficient liquid-liquid segregation to have occurred. This could explain the vertical meter-scale succession of apatite-Fe-Ti oxide ferrogabbros (nelsonite) and plagioclase-dominated leucogabbros present in the Bushveld Upper Zone.

Supplementary data to this article can be found online at <http://dx.doi.org/10.1016/j.lithos.2012.06.034>.

## Acknowledgments

This work has been funded by the Belgian Fund for Joint Research (FNRS) and the Natural Environment Research Council (NERC grant NE/F020325/1). ON acknowledges support from the Isaac Newton Trust, Trinity College, University of Cambridge. BC acknowledges support by a Marie Curie International Outgoing Fellowship within the 7th European Community Framework Programme. We thank SOQUEM, Inc. and the Ministère des Ressources Naturelles et de la

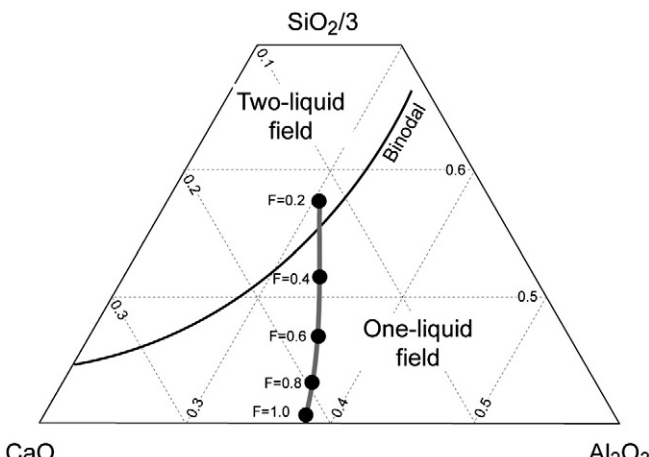


**Fig. 12.** The Bushveld Upper and Main Zone liquid compositions (Tegner et al., 2006) plotted on a section of the ternary diagram  $\text{SiO}_2/3\text{--CaO--Al}_2\text{O}_3$  (see Fig. 11b for details).

Faune du Québec for giving access to drill cores and unpublished geochemical data. J.L. Devidal and N. Delmelle provided assistance with electron microprobe and XRF analyses. Editorial handling by Andrew Kerr and detailed comments from two anonymous reviewers are highly appreciated and significantly improved the quality of the manuscript.

## References

- Bateman, A.M., 1951. The formation of late magmatic oxide ores. *Economic Geology* 46, 404–426.
- Bogaerts, M., Schmidt, M.W., 2006. Experiments on silicate melt immiscibility in the system  $\text{Fe}_2\text{SiO}_4$ – $\text{KAlSi}_3\text{O}_8$ – $\text{SiO}_2$ – $\text{CaO}$ – $\text{MgO}$ – $\text{TiO}_2$ – $\text{P}_2\text{O}_5$  and implications for natural magmas. *Contributions to Mineralogy and Petrology* 152, 257–274.
- Cawthorn, R.G., Ashwal, L.D., 2009. Origin of anorthositic and magnetitite layers in the Bushveld Complex, constrained by major element compositions of plagioclase. *Journal of Petrology* 50, 1607–1637.
- Charlier, B., Sakoma, E., Sauvé, M., Stanaway, K., Vander Auwera, J., Duchesne, J.C., 2008. The Grader layered intrusion (Havre-Saint-Pierre anorthositic, Quebec) and genesis of nelsonites and other Fe–Ti–P ores. *Lithos* 101, 359–378.
- Charlier, B., Namur, O., Toplis, M.J., Schiano, P., Cluzel, N., Higgins, M.D., Vander Auwera, J., 2011. Large-scale silicate liquid immiscibility during differentiation of basalt to granite and the origin of the Daly gap. *Geology* 39, 907–910.
- Charlier, B., Grove, T.L., 2012. Experiments on liquid immiscibility along tholeiitic liquid lines of descent. *Contributions to Mineralogy and Petrology* 164, 27–44.
- Dick, H.J.B., Natland, J.H., et al., 2000. A long *in situ* section of the lower ocean crust: results of ODP Leg 176 drilling at the Southwest Indian Ridge. *Earth and Planetary Science Letters* 179, 31–51.
- Dixon, S., Rutherford, M.J., 1979. Plagiogranites as late-stage immiscible liquids in ophiolite and mid-ocean ridge suites: an experimental study. *Earth and Planetary Science Letters* 45, 45–60.
- Duchesne, J.C., Charlier, B., 2005. Geochemistry of cumulates from the Bjerkreim–Sokndal layered intrusion (S. Norway). Part I: constraints from major elements on the mechanism of cumulate formation and on the jotunite liquid line of descent. *Lithos* 83, 229–254.
- Duchesne, J.C., Shumlyansky, L., Charlier, B., 2006. The Fedorivka layered intrusion (Korosten Pluton, Ukraine): an example of highly differentiated ferrobasaltic evolution. *Lithos* 89, 353–376.
- Dymek, R.F., Owens, B.E., 2001. Petrogenesis of apatite-rich rocks (nelsonites and oxide–apatite gabbronorites) associated with massif anorthosites. *Economic Geology* 96, 797–815.
- Eales, H.V., Cawthorn, R.G., 1996. The Bushveld Complex. In: Cawthorn, R.G. (Ed.), Layered intrusions : Developments of Petrology, 15. Elsevier, Amsterdam, pp. 181–230.
- Grove, T.L., Gerlach, D.C., Sando, T.W., 1982. Origin of calc-alkaline series lavas at Medicine Lake Volcano by fractionation, assimilation and mixing. *Contributions to Mineralogy and Petrology* 80, 160–182.
- Grove, T.L., Baker, M.B., 1984. Phase equilibrium controls on the tholeiitic versus calc-alkaline differentiation trends. *Journal of Geophysical Research* 89, 3253–3274.
- Grove, T.L., Juster, T.C., 1989. Experimental investigations of low-Ca pyroxene stability and olivine–pyroxene–liquid equilibria at 1-atm in natural basaltic and andesitic liquids. *Contributions to Mineralogy and Petrology* 103, 287–305.
- Harlov, D.E., Andersson, U.B., Förster, H.J., Nyström, J.O., Dulski, P., Broman, C., 2002. Apatite–monazite relations in the Kuruunavaara magnetite–apatite ore, northern Sweden. *Chemical Geology* 191, 47–72.
- Higgins, M.D., 1991. The origin of laminated and massive anorthositic, Sept Iles layered intrusion, Quebec, Canada. *Contributions to Mineralogy and Petrology* 106, 340–354.
- Higgins, M.D., 2005. A new interpretation of the structure of the Sept Iles Intrusive Suite, Canada. *Lithos* 83, 199–213.
- Higgins, M.D., Doig, R., 1986. Geochemical constraints on the processes that were active in the Sept Iles complex. *Canadian Journal of Earth Sciences* 23, 670–681.
- Higgins, M.D., van Breemen, O., 1998. The age of the Sept Iles layered mafic intrusion, Canada: implications for the late Neoproterozoic/Cambrian history of southeastern Canada. *Journal of Geology* 106, 421–431.
- Holness, M.B., Stripp, G., Humphreys, M.C.S., Veksler, I.V., Nielsen, T.F.D., Tegner, C., 2011. Silicate liquid immiscibility within the crystal mush: late-stage magmatic microstructures in the Skaergaard intrusion, East Greenland. *Journal of Petrology* 52, 175–222.
- Hoover, J.D., Irvine, T.N., 1978. Liquidus relations and Mg–Fe partitioning on part of the system  $\text{Mg}_2\text{SiO}_4$ – $\text{Fe}_2\text{SiO}_4$ – $\text{CaMgSi}_2\text{O}_6$ – $\text{CaFeSi}_2\text{O}_6$ – $\text{KAlSi}_3\text{O}_8$ – $\text{SiO}_2$ . *Carnegie Institution of Washington Yearbook* 77, 774–784.
- Howarth, R.J., 1998. Improved estimators of uncertainty in proportions, point-counting, and pass-fail test results. *American Journal of Science* 298, 594–607.
- Humphreys, M.C.S., 2011. Silicate liquid immiscibility within the crystal mush: evidence from Ti in plagioclase from the Skaergaard intrusion. *Journal of Petrology* 52, 147–174.
- Irvine, T.N., 1970. Heat transfer during solidification of layered intrusions. I. Sheets and sills. *Canadian Journal of Earth Sciences* 7, 1031–1061.
- Irvine, T.N., 1982. Terminology for layered intrusions. *Journal of Petrology* 23, 127–162.
- Jakobsen, J.K., Veksler, I.V., Tegner, C., Brooks, C.K., 2005. Immiscible iron- and silicate melts in basalt petrogenesis documented in the Skaergaard intrusion. *Geology* 33, 885–888.
- Jakobsen, J.K., Veksler, I.V., Tegner, C., Brooks, C.K., 2011. Crystallization of the Skaergaard intrusion from an emulsion of immiscible iron- and silica-rich liquids: evidence from melt inclusions in plagioclase. *Journal of Petrology* 52, 345–373.
- Jaupart, C., Brandeis, G., Allègre, C.J., 1984. Stagnant layers at the bottom of convecting magma chambers. *Nature* 308, 535–538.
- Kress, V.C., Carmichael, I.S., 1991. The compressibility of silicate liquids containing  $\text{Fe}_2\text{O}_3$  and the effect of composition, temperature, oxygen fugacity and pressure on their redox states. *Contributions to Mineralogy and Petrology* 108, 82–92.
- Kruger, F.J., Cawthorn, R.G., Walsh, K.L., 1987. Strontium isotopic evidence against magma addition in the Upper Zone of the Bushveld Complex. *Earth and Planetary Science Letters* 84, 51–58.
- Libourel, G., 1999. Systematics of calcium partitioning between olivine and silicate melt: implications for melt structure and calcium content of magmatic olivines. *Contributions to Mineralogy and Petrology* 136, 63–80.
- Loncarevic, B.D., Feininger, T., Lefevre, D., 1990. The Sept Iles layered mafic intrusion: geophysical expression. *Canadian Journal of Earth Sciences* 27, 501–512.
- Longhi, J., 1977. Magma oceanography 2: chemical evolution and crustal formation. *Proceedings of the Lunar Science Conference VIII*, pp. 601–621.
- Lundgaard, K.L., Tegner, C., 2004. Partitioning of ferric and ferrous iron between plagioclase and silicate melt. *Contributions to Mineralogy and Petrology* 147, 470–483.
- Martin, B., Kushiro, I., 1991. Immiscibility synthesis as an indication of cooling rates of basalts. *Journal of Volcanology and Geothermal Research* 45, 289–310.
- McBirney, A.R., 1975. Differentiation of the Skaergaard intrusion. *Nature* 253, 691–694.
- McBirney, A.R., 1996. The Skaergaard intrusion. In: Cawthorn, R.G. (Ed.). Layered intrusions. *Developments in Petrology* 15, 147–180.
- McBirney, A.R., Nakamura, Y., 1973. Immiscibility in late-stage magmas of the Skaergaard intrusion. *Carnegie Institution of Washington Geophysical Laboratory Report*, pp. 348–352.
- McBirney, A.R., Naslund, H.R., 1990. The differentiation of the Skaergaard intrusion, a discussion of Hunter and Sparks (*Contrib. Mineral. Petrol.* 95, 451–461). *Contributions to Mineralogy and Petrology* 104, 235–240.
- Miller, J.D., Ripley, E.M., 1996. Layered intrusions of the Duluth Complex, Minnesota, USA. In: Cawthorn, R.G. (Ed.), Layered intrusions. : *Developments of Petrology*, 15. Elsevier, Amsterdam, pp. 257–302.
- Namur, O., Charlier, B., Toplis, M.J., Higgins, M.D., Liégeois, J.P., Vander Auwera, J., 2010. Crystallization sequence and magma chamber processes in the ferrobasaltic Sept Iles layered intrusion, Canada. *Journal of Petrology* 51, 1203–1236.
- Namur, O., Charlier, B., Toplis, M.J., Higgins, M.D., Hounsell, V., Liégeois, J.P., Vander Auwera, J., 2011a. Continuous differentiation of tholeiitic basalt to A-type granite in the Sept Iles layered intrusion, Canada. *Journal of Petrology* 52, 487–539.
- Namur, O., Charlier, B., Pirard, C., Hermann, J., Liégeois, J.P., Vander Auwera, J., 2011b. Anorthosite formation by plagioclase flotation in ferrobasalt and implications for the lunar crust. *Geochimica et Cosmochimica Acta* 75, 4998–5018.
- Namur, O., Charlier, B., 2012. Efficiency of compaction and compositional convection during mafic crystal mush solidification: the Sept Iles layered intrusion, Canada. *Contributions to Mineralogy and Petrology* 163, 1049–1068.
- Namur, O., Charlier, B., Toplis, M.J., Vander Auwera, J., 2012. Prediction of plagioclase-melt equilibria in anhydrous silicate melts at 1-atm. *Contributions to Mineralogy and Petrology* 163, 133–150.
- Naslund, H.R., 1983. The effect of oxygen fugacity on liquid immiscibility in iron-bearing silicate melts. *American Journal of Science* 283, 1034–1059.
- Natland, J.H., Meyer, P.S., Dick, H.J.B., et al., 1991. Magmatic oxides and sulphides in gabbroic rocks from Hole 735B and the later development of the liquid line of descent. In: Von Herzen, R.P., Robinson, P.T., et al. (Eds.), *Proceedings of ODP Scientific Results*, 118. Ocean Drilling Program, College Station, TX, pp. 75–111.
- Philpotts, A.R., 1967. Origin of certain iron-titanium oxide and apatite rocks. *Economic Geology* 62, 303–315.
- Philpotts, A.R., Doyle, C.D., 1983. Effect of magma oxidation state on the extent of silicate liquid immiscibility in a tholeiitic basalt. *American Journal of Science* 283, 967–986.
- Putirka, K.D., 2008. Thermometers and barometers from volcanic systems. In: Putirka, K.D., Tepley, F.J. (Eds.), Minerals, inclusions and volcanic processes: *Reviews in Mineralogy and Petrology*, 69, pp. 61–120.
- Ripley, E.M., Severson, M.J., Hauck, S.E., 1998. Evidence for sulfide and Fe–Ti–P rich liquid immiscibility in the Duluth Complex, Minnesota. *Economic Geology* 93, 1052–1062.
- Roedder, E., 1951. Low temperature liquid immiscibility in the system  $\text{K}_2\text{O}$ – $\text{FeO}$ – $\text{Al}_2\text{O}_3$ – $\text{SiO}_2$ . *American Mineralogist* 36, 282–286.
- Roedder, E., 1978. Silicate liquid immiscibility in magmas and in the system  $\text{K}_2\text{O}$ – $\text{FeO}$ – $\text{Al}_2\text{O}_3$ – $\text{SiO}_2$ : an example of serendipity. *Geochimica et Cosmochimica Acta* 42, 1597–1617.
- Shi, P., 1993. Low-pressure phase relationships in the system  $\text{Na}_2\text{O}$ – $\text{CaO}$ – $\text{FeO}$ – $\text{MgO}$ – $\text{Al}_2\text{O}_3$ – $\text{SiO}_2$  at 1100°C, with implications for the differentiation of basaltic magmas. *Journal of Petrology* 34, 743–762.
- Tegner, C., Cawthorn, R.G., Kruger, F.J., 2006. Cyclicity in the Main and Upper Zones of the Bushveld Complex, South Africa: crystallization from a zoned magma sheet. *Journal of Petrology* 47, 2257–2279.
- Thy, P., Leshner, C.E., Nielsen, T.F., Brooks, C.K., 2006. Experimental constraints on the Skaergaard liquid line of descent. *Lithos* 92, 154–180.
- Thy, P., Leshner, C.E., Tegner, C., 2009. The Skaergaard liquid line of descent revisited. *Contributions to Mineralogy and Petrology* 157, 735–747.
- Tollari, N., Toplis, M.J., Barnes, S.J., 2006. Predicting phosphate saturation in silicate magmas: an experimental study of the effects of melt composition and temperature. *Geochimica et Cosmochimica Acta* 70, 1518–1536.
- Tollari, N., Barnes, S.J., Cox, R.A., Nabil, H., 2008. Trace element concentrations in apatites from the Sept Iles Intrusive Suite, Canada: implications for the genesis of nelsonites. *Chemical Geology* 252, 180–190.

- Toplis, M.J., 2005. The thermodynamics of iron and magnesium partitioning between olivine and liquid: criteria for assessing and predicting equilibrium in natural and experimental systems. *Contributions to Mineralogy and Petrology* 149, 22–39.
- Toplis, M.J., Libourel, G., Carroll, M.R., 1994. The role of phosphorous in crystallization processes of basalt: an experimental study. *Geochimica et Cosmochimica Acta* 58, 797–810.
- Toplis, M.J., Carroll, M.R., 1995. An experimental study of the influence of oxygen fugacity on Fe–Ti oxide stability, phase relations, and mineral–melt equilibria in ferro-basaltic systems. *Journal of Petrology* 36, 1137–1170.
- Toplis, M.J., Carroll, M.R., 1996. Differentiation of ferro-basaltic magmas under conditions open and closed to oxygen: implications for the Skaergaard intrusion and other natural systems. *Journal of Petrology* 37, 837–858.
- Van Tongeren, J.A., Mathez, E.A., Kelemen, P.B., 2010. A felsic end to the Bushveld differentiation. *Journal of Petrology* 51, 1891–1912.
- Van Tongeren, J.A., Mathez, E.A., 2012. Large-scale liquid immiscibility at the top of the Bushveld Complex, South Africa. *Geology* 20, 491–494.
- Veksler, I.V., 2009. Extreme iron enrichment and liquid immiscibility in mafic intrusions: experimental evidence revisited. *Lithos* 111, 72–82.
- Visser, W., Koster van Groos, A.F., 1979a. Phase relations in the system  $K_2O$ – $FeO$ – $Al_2O_3$ – $SiO_2$  at 1 atmosphere with special emphasis on low temperature liquid immiscibility. *American Journal of Science* 279, 70–91.
- Visser, W., Koster van Groos, A.F., 1979b. Effect of  $P_2O_5$  and  $TiO_2$  on liquid–liquid equilibria in the system  $K_2O$ – $FeO$ – $Al_2O_3$ – $SiO_2$ . *American Journal of Science* 279, 970–988.
- Wager, L.R., Brown, G.M., 1968. Layered Igneous Rocks. Oliver & Boyd, London. (588 pp.).
- Watson, E.B., 1976. Two-liquid partition coefficients: experimental data and geochemical implications. *Contributions to Mineralogy and Petrology* 56, 119–134.
- Zhao, T.-P., Chen, W., Zhou, M.-F., 2009. Geochemical and Nd–Hf isotopic constraints on the origin of the 1.74-Ga Damiao anorthosite complex, North China Craton. *Lithos* 113, 673–690.
- Zhou, M.-F., Robinson, P.T., Lesher, C.M., Keays, R.R., Zhang, C.-J., Malpas, J., 2005. Geochemistry, petrogenesis and metallogenesis of the Panzhihua gabbroic layered intrusion and associated Fe–Ti–V oxide deposits, Sichuan Province, SW China. *Journal of Petrology* 46, 2253–2280.